

D2.3 – Uncertainty quantification approach and computational uncertainties associated with each research reactor

Version n°0.2

August/2026

Yann Périn[1], Mathieu Hursin[2], Klemen Ambrožič[3,4]

1. Gesellschaft für Anlagen- und Reaktorsicherheit (GRS) gGmbH, Germany
2. Laboratory for Reactor Physics and Systems Behavior, EPFL - Swiss Federal Technology Institute of Lausanne, Switzerland
3. Reactor Physics Division, Jožef Stefan Institute, Slovenia
4. Faculty of Mathematics and Physics, University of Ljubljana, Slovenia

Funded by the European Union

Funded by the European Union. Views and opinions expressed are however those of the author(s) only and do not necessarily reflect those of the European Union or the European Atomic Energy Community ('EC-Euratom'). Neither the European Union nor the granting authority can be held responsible for them.

Disclaimer

Funded by the European Union. Views and opinions expressed are however those of the author(s) only and do not necessarily reflect those of the European Union or the European Atomic Energy Community ('EC-Euratom'). Neither the European Union nor the granting authority can be held responsible for them.

Funded by the European Union
Funded by the European Union. Views and opinions expressed are however those of the author(s) only and do not necessarily reflect those of the European Union or the European Atomic Energy Community ('EC-Euratom'). Neither the European Union nor the granting authority can be held responsible for them.

Document information

Grant Agreement	n°101163288
Project Title	Experiments for Validation and Enhancement of the REactor preSsure vessel fluence assessmenT
Project Acronym	EVEREST
Project Coordinator	Yann Perin – GRS
Project Duration	01.09.2024 – 30.09.2028 (48 months)
Related Work Package	WP2
Related Task(s)	T 2.3
Lead Organisation	GRS
Contributing Partner(s)	JSI, GRS, EPFL
Due Date	September 1st, 2026
Submission Date	August 31st, 2026
Dissemination level	PU

History

Date	Version	Submitted by	Reviewed by	Comments
28.08.26	0.1	Y. Perin	M. Hursin	Initial
31.08.26	0.2	K. Lavoisier	Y. Perin L. Duivon	Final

Funded by the European Union

Funded by the European Union. Views and opinions expressed are however those of the author(s) only and do not necessarily reflect those of the European Union or the European Atomic Energy Community ('EC-Euratom'). Neither the European Union nor the granting authority can be held responsible for them.

Table of contents

1 Introduction 11
1.1 Objectives 11
1.2 Scope 11
2 Methodology 12
2.1 Uncertainty quantification approach at GRS 12
2.1.1 SUSA 12
2.1.2 XSUSA 13
2.2 Uncertainty quantification approach at EPFL 14
2.2.1 Sampling of nuclear data uncertainty with the NUSS tool 14
2.2.2 Sampling of technological and thermal-hydraulic parameters 14
2.2.3 Sensitivity analysis (SA) 14
3 Computational uncertainties associated with each research reactor 16
3.1 BME Training Reactor 16
3.1.1 GRS Uncertainty Analysis 16
3.1.1.1 Model description 16
3.1.1.2 Nuclear data uncertainties 16
3.1.1.3 Other sources of uncertainty 16
3.1.1.4 Preliminary assessment of the uncertainty 18
3.1.2 EPFL Uncertainty Analysis 19
3.1.2.1 TRACE/PARCS model description 19
3.1.2.2 Nuclear data uncertainties 20
3.1.2.3 Technological uncertainties 20
3.1.2.4 Preliminary assessment of the uncertainty 22
3.2 Budapest Research Reactor 28
3.2.1 Nuclear data uncertainties 28
3.2.2 UQ/SA Methodology 28
3.2.3 Results 29
3.2.3.1 Quantities of Interest 29
3.2.3.2 Computational uncertainty due to Monte Carlo statistics 29
3.2.3.3 k_{eff} Uncertainty 30
3.2.3.4 2D Core Power Distribution 31
3.2.3.5 Axial Dosimetry-Response and Flux Uncertainties at the Fast Flux Trap 32
3.2.3.6 Uncertainty Due to IRDFF Dosimetry Cross Sections 34
3.2.3.7 Radial Variation at the Flux Trap 35

Funded by the European Union

Funded by the European Union. Views and opinions expressed are however those of the author(s) only and do not necessarily reflect those of the European Union or the European Atomic Energy Community ('EC-Euratom'). Neither the European Union nor the granting authority can be held responsible for them.

3.3 JSI TRIGA reactor 36
3.3.1 JSI Uncertainty Analysis 37
3.3.2 GRS Uncertainty Analysis 38
3.3.2.1 Model description 38
3.3.2.2 Nuclear data uncertainties 38
3.3.2.3 Other sources of uncertainty 39
3.3.2.4 Preliminary assessment of the uncertainty 40
4 Conclusions and further work 43

Funded by the European Union

Funded by the European Union. Views and opinions expressed are however those of the author(s) only and do not necessarily reflect those of the European Union or the European Atomic Energy Community ('EC-Euratom'). Neither the European Union nor the granting authority can be held responsible for them.

List of figures

Figure 1: BME Training reactor core with position of analysed locations 18
Figure 2: Average flux in the 7 energy groups for 4 selected pins. 19
Figure 3: Standard deviation of the flux in 7 energy groups for 4 selected pins 19
Figure 4: Relative covariance matrix (%) of the fuel isotopic composition. 22
Figure 5: Convergence of the mean rod worth for the MAN and AUT control rods. 23
Figure 6: Distribution of rod worth samples. 24
Figure 7: Contributor to the ARO keff uncertainty, ranked by GRS sensitivity index The convergence with the number of samples is also represented. 25
Figure 8: Evolution of the power computational uncertainty with time during the FB#2 transient. ... 26
Figure 9: Main contributors to the power uncertainty during the FB#2 transient. 26
Figure 10: Evolution of the temperature computational uncertainty at the exit of the C7 channel, with time during the FB#2 transient. 27
Figure 11: Main contributors to the temperature uncertainty at the exit of the C7 channel, during the FB#2 transient. 27
Figure 12: Effect of the Monte Carlo uncertainties in the macroscopic library generation process, on the transient uncertainties. 28
Figure 13: Importance map used during the fixed source Serpent2 calculations. 29
Figure 14: Nuclear-data-driven k_{eff} uncertainty for the sampled configurations. 31
Figure 15: Mean and relative-standard-deviation maps for the 2D core power distribution. 32
Figure 16: Axial variation and sensitivity indices for the Au-197 (n,g) response at the fast flux trap. . 32
Figure 17: Axial variation and sensitivity indices for the Fe-58 (n,g) response at the fast flux trap. 33
Figure 18: Axial variation for the Fe-54 (n,p) response at the fast flux trap. 33
Figure 19: Sensitivity indices for the Fe-54 (n,p) response at the fast flux trap. 34
Figure 20: Fe-54 (n,p) threshold region overlaid on the U-235 fission-spectrum uncertainty, explaining the large propagated uncertainty. 34
Figure 21: Mean axial reaction-rate profiles (±1σ sample spread) and relative standard deviation, from IRDFF-II dosimetry cross-section perturbations. 35
Figure 22: Mean and relative standard deviation of a mesh tally covering the flux-trap location for the Fe-58 (n,g) reaction rates. 35
Figure 23: Mean and relative standard deviation of a mesh tally covering the flux-trap location for the Au-197 (n,g) reaction rates. 36
Figure 24: Mean and relative standard deviation of a mesh tally covering the flux-trap location for the Fe-54 (n,p) reaction rates. 36
Figure 25: JSI TRIGA core with position of analysed locations 40
Figure 26: Average flux in the 2 energy groups for 5 selected pins 41
Figure 27: Relative standard deviation of the flux in 2 energy groups for 5 selected pins 41
Figure 28: Average stochastic uncertainty of the flux in 2 energy groups for 5 selected pins 42

Funded by the European Union

Funded by the European Union. Views and opinions expressed are however those of the author(s) only and do not necessarily reflect those of the European Union or the European Atomic Energy Community ('EC-Euratom'). Neither the European Union nor the granting authority can be held responsible for them.

List of tables

Table 1: Manufacturing Uncertainties 17
Table 2: Core Boundary Condition Standard Deviations 17
Table 3: Material properties recommended uncertainties 18
Table 4: Technological and thermal-hydraulic uncertain input parameters and their assumed distributions. 21
Table 5: Mean keff and its standard deviation (in pcm) for the BME reactor configurations. 23
Table 6: Mean rod worth and its standard deviation (in $) for the BME reactor configurations. 24
Table 7: Monte Carlo statistical spread, from the random-seed study (nominal nuclear data)..... 30
Table 8: Relative standard deviation attributable to IRDFF-II dosimetry cross-section uncertainty alone. 35
Table 9: Radial spread of dosimetry reaction rates around the nominal position within the flux trap. 36
Table 10: Summary of Modelling Uncertainties by Experiment 38
Table 11: Manufacturing Uncertainties 39
Table 12: Core Boundary Condition Standard Deviations 39
Table 13: Material properties recommended uncertainties 39

Funded by the European Union

Funded by the European Union. Views and opinions expressed are however those of the author(s) only and do not necessarily reflect those of the European Union or the European Atomic Energy Community ('EC-Euratom'). Neither the European Union nor the granting authority can be held responsible for them.

Summary

The primary objective of WP2 is to produce validated advanced multi-physics computational models for the research reactors involved in the project: the BRR at HUN-REN EK, the TR at BME, and the TRIGA Mark II at JSI. This deliverable focuses specifically on describing the methods and approaches applied in Task 2.3: Uncertainty quantification of research reactor conventional models.

This task aims at quantifying the computational uncertainties of the conventional model of each research reactor experiment. For this purpose, existing frameworks available at EPFL and GRS are implemented to determine the computational uncertainties associated with the quantities of interest e.g., the neutron flux and temperature at the measurement locations. Both frameworks rely on statistical methods. The uncertainties associated with the nuclear data as well as the technological parameters (fuel compositions, geometry, etc...) and boundary conditions are considered. The random output samples will be useful for the assessment of the discrepancies between codes and measurements in Task 2.4; as well as the representativity of the research reactors to a nuclear power plant.

This report covers uncertainty quantification pipelines developed for the three research reactors involved in WP2: the Budapest Research Reactor (BRR), the BME Training Reactor (TR), and the JSI TRIGA Mark II reactor. For each facility, the uncertainty quantification work encompasses the uncertainty from the nuclear data, the thermal-hydraulics parameters, technological parameters as well as modelling parameters of the coupled multi-physics problem.

For the BME TR, the GRS approach, which couples the neutronics code FENNECS with the thermal-hydraulics subchannel code CTF in an open-core representation, focuses on thermal-hydraulics and nuclear data uncertainties following the UAM-LWR benchmark methodology. At this point, the uncertainty quantification is limited to the nuclear data uncertainty on the HELIOS model which is used for the cross-section generation. For this preliminary study, 100 samples are computed and analysed.

In the EPFL approach, based on the Serpent2/TRACE/PARCS calculation scheme, nuclear data uncertainties and technological parameters uncertainties are propagated through a 300-sample ensemble to assess the steady-state reactivity, control-rod worths, and the FB#2 transient response

For the BRR, the propagation of uncertainties currently covers mainly nuclear data uncertainties as the model relies of the Serpent2 input developed in D2.2. Such choice is supported by the limited impact of temperature feedback reported in that document.

For the JSI TRIGA reactor, the GRS approach is the same as for the BME pipeline except for the cross-section generation tool which is switched from HELIOS to Serpent 2. At this point, the uncertainty quantification is limited to the nuclear data uncertainty on the Serpent 2 model which is used for the cross-section generation. For this preliminary study, 100 samples were computed and analysed. In some cases, the stochastic can no longer be neglected in front of the nuclear data uncertainty. In further analyses, the statistics of the Monte Carlo simulation will be improved in order to minimize this effect. Furthermore, a summary of previous work carried out at JSI to quantify computational uncertainties is presented.

Funded by the European Union

Funded by the European Union. Views and opinions expressed are however those of the author(s) only and do not necessarily reflect those of the European Union or the European Atomic Energy Community ('EC-Euratom'). Neither the European Union nor the granting authority can be held responsible for them.

Keywords

Uncertainty quantification, sensitivity analysis, multi-physics, TRIGA, BME Training Reactor, Budapest Research Reactor

Abbreviations and acronyms

Acronym	Description
WP	Work Package
BRR	Budapest Research Reactor
BME	Budapest University of Technology and Economics
JSI	Jožef Stefan Institute
MC	Monte Carlo
MP	Multi-Physics
QoI	Quantity of Interest
TRIGA	Training Research Isotope production by General Atomics
WP	Work Package

Funded by the European Union

Funded by the European Union. Views and opinions expressed are however those of the author(s) only and do not necessarily reflect those of the European Union or the European Atomic Energy Community ('EC-Euratom'). Neither the European Union nor the granting authority can be held responsible for them.

1 Introduction

The safety of nuclear reactors relies heavily on modelling, and the accuracy of those models is only as reliable as the experimental data used to validate them. Over the past two decades, advanced multi-physics (MP) simulation platforms have been developed to reduce the level of conservatism inherent in conventional reactor modelling approaches. Unlike the traditional two-step, assembly-level methods that rely on pin-power reconstruction schemes, these advanced tools apply a first-principles approach and deliver solutions at a much finer spatial resolution without the need for intermediate reconstruction. Despite this improved capability, advanced MP codes remain seldom used in practice, in part because dedicated, high-resolution experimental data for their validation are scarce.

The EVEREST project (Experiments for Validation and Enhancement of the REactor preSsure vessel fluence assessmenT, Grant Agreement n°101163288) was established under the Euratom Research and Training Programme to address this gap. The project focuses on three complementary objectives: quantifying the added value of advanced MP models for long-term operation (LTO) applications and reactor pressure vessel (RPV) fluence assessment; demonstrating the trustworthiness of these models through the production of dedicated experimental data; and promoting their adoption among key stakeholders in the nuclear engineering community, including utilities, regulators, and students.

Work Package 2 (WP2) of the EVEREST project is specifically dedicated to the production of validated high-resolution multi-physics models of these research reactors, with EPFL as work package leader. The present document, Deliverable D2.3, reports on the uncertainty quantification frameworks developed for each of the three research reactors involved in WP2.

1.1 Objectives

The primary objective of WP2 is to produce validated advanced multi-physics computational models for the research reactors involved in the project: the BRR at HUN-REN EK, the TR at BME, and the TRIGA Mark II at JSI. This deliverable focuses specifically on describing the methods and approaches applied in Task 2.3: Uncertainty quantification of research reactor conventional models.

This task aims at quantifying the computational uncertainties of the conventional model of each research reactor experiment. For this purpose, existing frameworks available at EPFL and GRS are implemented to determine the computational uncertainties associated with the quantities of interest e.g., the neutron flux and temperature at the measurement locations. Both frameworks rely on statistical methods. The uncertainties associated with the nuclear data as well as the technological parameters (fuel compositions, geometry, etc...) and boundary conditions are considered. The random output samples will be useful for the assessment of the discrepancies between codes and measurements in Task 2.4; as well as the representativity of the research reactors to a nuclear power plant.

1.2 Scope

This report covers uncertainty quantification pipelines developed for the three research reactors involved in WP2: the Budapest Research Reactor (BRR), the BME Training Reactor (TR), and the JSI TRIGA Mark II reactor. For each facility, the uncertainty quantification work encompasses the uncertainty from the nuclear data, the thermal-hydraulics parameters, technological parameters as well as modelling parameters of the coupled multi-physics problem.

Funded by the European Union

Funded by the European Union. Views and opinions expressed are however those of the author(s) only and do not necessarily reflect those of the European Union or the European Atomic Energy Community ('EC-Euratom'). Neither the European Union nor the granting authority can be held responsible for them.

2 Methodology

2.1 Uncertainty quantification approach at GRS

2.1.1 SUSA

A widely used and effective approach for quantifying the uncertainty of a computational result, or figure of merit, is the Monte Carlo (MC) simulation method. This technique is based on the characterization of uncertainties associated with relevant input parameters and their propagation through a computational model. In practice, values for uncertain input parameters are randomly sampled according to their specified uncertainty distributions and used as inputs for repeated model evaluations. The resulting set of output values is then statistically analyzed to derive meaningful measures of the uncertainty associated with the computational result.

To determine which uncertainty sources have the greatest impact on the output, a complementary global sensitivity analysis can be performed. Such an analysis helps identify the parameters that contribute most significantly to the overall uncertainty and indicates where improved knowledge or data would be most effective in reducing uncertainty.

To support uncertainty and sensitivity analyses based on Monte Carlo simulation, the software tool SUSA (Software for Uncertainty and Sensitivity Analyses) (Horst Glaeser, 2008) was developed. SUSA integrates established methods from probability theory and statistics within a user-friendly graphical user interface (GUI). Its design allows users to focus on defining the analysis inputs, including identifying the key uncertain parameters and specifying their associated uncertainties. Once these elements have been established, SUSA assists in the probabilistic quantification of uncertainties and guides users through the various stages of uncertainty and sensitivity analysis.

The main steps of a probabilistic uncertainty and sensitivity analysis supported by SUSA can be summarized as follows:

1- Identification of the uncertain input parameters which may essentially contribute to the uncertainty of the computational result.
2- Document and quantify the uncertainty of the parameters in terms of univariate probability distributions and dependences (e.g. association measures, conditional distributions, or functional relationships).
3- SUSA generates a sample of values for the parameters based on the quantifications made in step 2.
4- Run the corresponding computer code for the sets of parameter values sampled in step 3 and extract the relevant values from the computational results.
5- SUSA calculates statistics useful for quantifying the uncertainty of the computational results.
6- SUSA calculates sensitivity indices and provides a ranking of the parameters with respect to their contribution to the uncertainty of the computational results.

Using this approach, the number of runs becomes independent from the number of uncertain parameters and no a priori ranking is necessary. The minimum required number ‘n’ of simulations is given by the Wilks’ formula in which ‘n’ only depends on two parameters:

- The probability ‘a’ × 100 (%) (or percentile) of the output distribution

- The confidence level ‘b’ × 100 (%) that the maximum code result will not be exceeded

The Wilks’ formula for a two-sided tolerance limit is: $1-a^n-n(1-a)a^{n-1} \geq b$

Funded by the European Union

Funded by the European Union. Views and opinions expressed are however those of the author(s) only and do not necessarily reflect those of the European Union or the European Atomic Energy Community ('EC-Euratom'). Neither the European Union nor the granting authority can be held responsible for them.

For example, applying the formula with a 95th percentile value with a confidence level of 95% for a two-sided tolerance limit, one obtains a minimum number of simulation n = 93.

It is important to note that more runs may be necessary for a relevant sensitivity analysis.

2.1.2 XSUSA

Within the sampling-based GRS methodology implemented in the SUSA package, a large number of calculations are performed using systematically varied input data. The GRS method was originally developed and primarily applied to problems involving a relatively small number of uncertain parameters and only limited correlations, such as thermal-hydraulics and technological variables.

However, its extension to nuclear data uncertainty analysis through XSUSA (Aures et al., 2025; Bousquet et al., 2018) presents a much greater level of complexity. When nuclear covariance data from the SCALE 6 code package are used, 44 uncertain parameters are considered for each nuclide-reaction pair, corresponding to the 44-group energy structure. This leads to a very large total number of uncertain parameters. In addition, significant correlations must be accounted for, including correlations among energy groups within a given nuclide-reaction combination as well as cross-correlations between different reactions and nuclides.

The nuclear covariance matrices provide only the relative variances and covariances of the nuclear data, representing the second-order moments of the underlying distributions. Since the actual distribution types are not explicitly specified, they are assumed to follow Gaussian distributions. To apply the GRS methodology using these covariance data, either the original ENDF/B-VII-based 238-group SCALE 6 library is employed directly, or it is collapsed into the 44-group covariance structure using a flux spectrum representative of the system under study. The latter approach can be particularly advantageous for full-core analyses, where large quantities of data associated with numerous fuel assemblies and burnup states must be managed efficiently.

Using either the original or the collapsed master library, all required spectral calculations are carried out. The resulting problem-specific cross-section libraries are then modified according to the uncertainty information contained in the covariance matrices for each considered nuclide-reaction pair. Following these modifications, the consistency of the complete cross-section set must be verified. In particular, all relevant sum rules must remain satisfied, and multidimensional cross sections, such as scattering matrices, must be consistent with their corresponding one-dimensional representations.

Recently, XSUSA was further extended to include the variation of cross-section data in a continuous-energy representation in order to capture the impact of nuclear data uncertainties on the results of Monte Carlo neutron transport calculations. This extension, called XSUSA-CE, made the advantages of Monte Carlo neutron transport methods over deterministic approaches available for uncertainty analyses, namely the use of continuous-energy cross-section data and the modeling of complex nuclear geometries without significant approximations.

Continuous-energy cross-section data in the ACE format commonly used by the Monte Carlo code Serpent are varied using a sampling-based approach based on multigroup covariance data from SCALE 6.2. Prior to this, the ACE data are augmented to ensure that data points are available within every energy interval of the covariance data, thereby enabling a consistent variation process. In addition, sum rules are enforced; that is, for example, a variation of the elastic scattering cross section also requires a corresponding variation of the total cross section.

To validate the method, sensitivity profiles of the multiplication factor with respect to the varied cross sections were determined for several critical experiments by directly varying the cross-section data.

Funded by the European Union

Funded by the European Union. Views and opinions expressed are however those of the author(s) only and do not necessarily reflect those of the European Union or the European Atomic Energy Community ('EC-Euratom'). Neither the European Union nor the granting authority can be held responsible for them.

The resulting sensitivity profiles showed acceptable agreement with reference results obtained using TSUNAMI and Serpent's built-in sensitivity analysis method.

2.2 Uncertainty quantification approach at EPFL

The UQ approach used at EPFL relies on simple random sampling: a set of *N* (independent or correlated) samples of the uncertain inputs is drawn, each sample is propagated through the full calculation chain, and the resulting ensemble of output values is used to estimate the mean, standard deviation and, where relevant, the sensitivity of each quantity of interest. Unless otherwise noted, the sample size is set to 300 to reduce the statistical noise on the sensitivity indices discussed in Section 3.1.2.

2.2.1 Sampling of nuclear data uncertainty with the NUSS tool

The nuclear data part of the input uncertainty is sampled with the NUSS tool developed at PSI (Zhu et al., 2015). For each random sample, NUSS draws a consistent set of perturbation factors for the isotope-reaction pairs from the ENDF/B-VII.1 19-energy-group variance-covariance matrix, and applies them to generate a randomly perturbed, ACE-formatted nuclear data library. Each perturbed ACE library is then used as input to the lattice/core neutronics calculations (Serpent2 and the PARCS few-group cross-section libraries derived from it), so that the propagated nuclear data uncertainty is fully consistent with the correlations encoded in the covariance matrix: the covariance information is used directly to perturb the evaluated data, rather than determining sensitivity coefficients and using the Sandwich formula.

2.2.2 Sampling of technological and thermal-hydraulic parameters

For the technological and thermal-hydraulic parameters (see the RR specific sections below for the list of considered uncertain input parameters), no equivalent covariance-driven tool was available, so a dedicated Python script was developed to generate the corresponding randomly perturbed input parameters of the research reactor model considered. For each of the *N* samples, the script draws one realization of each parameter from its assumed distribution and writes out a modified input of the model reflecting that realization, keeping the sample index consistent with the corresponding NUSS-perturbed nuclear data library so that the ND and TH perturbations are propagated together through the coupled calculation for that sample.

2.2.3 Sensitivity analysis (SA)

For the purpose of identifying the inputs responsible for the computational uncertainty, the use of an adequate SA method based on random samples is sought. Even though UQ is straightforward through the use of random sampling, SA based on those random samples is difficult due to the potential non-linearity of the model, to the large number of inputs, as well as to their correlations. In this work, SA is performed with a regression-based approach, often referred to as the "GRS method," applied directly to the input and output samples of the random-sampling calculations. No additional code runs beyond those already needed for the UQ study are required.

For each scalar input xi and output Y, the Pearson correlation coefficient r_p between the input samples and the output samples is computed. Under the assumption of a linear relationship between x_i and Y, the squared Pearson coefficient r_p^2 is the coefficient of determination of that linear relationship, i.e. the fraction of the variance of Y explained by a linear fit on x_i alone. This quantity is used directly as an estimator of the first-order sensitivity index of Y to x_i:

Funded by the European Union

Funded by the European Union. Views and opinions expressed are however those of the author(s) only and do not necessarily reflect those of the European Union or the European Atomic Energy Community ('EC-Euratom'). Neither the European Union nor the granting authority can be held responsible for them.

$$S_{xi} \approx r_p^2 (x_i, Y) \quad (1)$$

The approach generalizes to groups of correlated input parameters (for instance, all 19 energy groups of a given isotope-reaction pair) through the multiple correlation coefficient computed from the vector of correlation coefficients between the output and each member of the group, combined with the inverse of the group's sample covariance matrix (H. Glaeser et al., 2008).

Assuming a group of parameters $X_{(1)}=(X_1,\ldots,X_k)$, the multiple correlation coefficient $R^2_{(1)}$ is defined as Eq (2).

$$R^2_{(1)} = \left(\rho(Y,X_1),\ldots,\rho(Y,X_k)\right)\Sigma^{-1}_{X(1)}\left(\rho(Y,X_1),\ldots,\rho(Y,X_k)\right)^T \quad (2)$$

Where $\rho(Y,X_i)$ is the correlation coefficient between Y and xi. $\Sigma^{-1}_{X(1)}$ is the inverse of the VCM for the group of parameters $X_{(1)}$. The first order sensitivity index for a group of parameters can be defined as:

$$S_{X_{(1)}} = R^2_{X_{(1)}} \quad (3)$$

The VCM is estimated using the covariance of the input samples. The total sensitivity index obtained using this formula can be extended to determine the total sensitivity index of a single parameter x_i. In this case, $X_{(2)}$ represents all the input parameters but the one for which the sensitivity index is determined. It should be noted here that the number of samples *N* considered for the determination of the correlations and determination coefficients should be bigger than the number of input parameters *k* considered in any subset of input parameters.

This regression-based approach is attractive because it is computationally cheap, it reuses the N sample evaluations already produced for the UQ study, irrespective of the number of uncertain inputs. Moreover it makes no assumption about the shape of the input or output probability distributions. Its main limitation is that it assumes a linear relationship between each input and the output, an assumption that should be checked whenever the estimated sensitivity indices are used to draw conclusions about the underlying physics. This is the method used to produce the sensitivity index rankings and convergence plots discussed in Sections 3.1.2.4 and 3.2.3.

Funded by the European Union

Funded by the European Union. Views and opinions expressed are however those of the author(s) only and do not necessarily reflect those of the European Union or the European Atomic Energy Community ('EC-Euratom'). Neither the European Union nor the granting authority can be held responsible for them.

3 Computational uncertainties associated with each research reactor

3.1 BME Training Reactor

This section presents the uncertainty quantification analyses performed on the BME Training Reactor model by two independent partners, GRS and EPFL, each relying on a distinct computational chain. Section 3.1.1 describes the GRS approach, which couples the neutronics code FENNECS with the thermal-hydraulics subchannel code CTF in an open-core representation, focusing on thermal-hydraulics and nuclear data uncertainties following the UAM-LWR benchmark methodology. Section 3.1.2 presents the EPFL approach, based on the Serpent2/TRACE/PARCS calculation scheme, in which nuclear data uncertainties and technological parameters uncertainties are propagated through a 300-sample ensemble to assess the steady-state reactivity, control-rod worths, and the FB#2 transient response.

3.1.1 GRS Uncertainty Analysis

3.1.1.1 Model description

A brief description of the models is provided in this paragraph; a more complete description of the models and results can be found in D2.2 (Hursin et al., 2026).

The GRS model focuses on the core (open-core representation), wherein the neutronics code FENNECS is coupled with the thermal-hydraulics subchannel code CTF. The rest of the reactor pool is not modelled. Instead, the inlet mass flow and temperatures are given as boundary conditions.

HELIOS-2 is used for the generation of cross-section libraries for FENNECS. A lattice calculation is performed for the full core 2D geometry, condensed to seven energy groups and homogenised region by region (pin-wise and assembly-wise).

3.1.1.2 Nuclear data uncertainties

Applying XSUSA pre-generated perturbed nuclear data libraries in conjunction with the HELIOS model of the BME Training Reactor core, perturbed cross-section libraries for FENNECS are generated.

The isotope selection is composed of every isotope present in the nominal HELIOS model of the BME TR with a large enough concentration for which XSUSA provides perturbed nuclear data. Other isotopes in the model without an associated perturbed library are therefore not perturbed, and are implicitly treated as exactly known in this study. The isotopes list is the following:

- H-1, H-2, B-10, B-11, C-6, O-16, O-17, Mg-24, Mg-15, Mg-26, Al-27, Fe- 56, Cd-112, Cd-114, U-234, U-235, U-236, U-238, Pu-239, Pu-240

3.1.1.3 Other sources of uncertainty

The experience from the Uncertainty (UAM-LWR) benchmark from the OECD/NEA (Bratton et al., 2014) is used as basis for selecting the uncertain parameters as well as their uncertainty range. Various sources of uncertainties are examined such as modelling uncertainties, boundary condition uncertainties, and geometry/manufacturing uncertainties.

a) Uncertainties in manufacturing tolerances:
   - Cladding outside diameter,
   - Cladding thickness,
   - Cladding roughness,

Funded by the European Union

Funded by the European Union. Views and opinions expressed are however those of the author(s) only and do not necessarily reflect those of the European Union or the European Atomic Energy Community ('EC-Euratom'). Neither the European Union nor the granting authority can be held responsible for them.

- Fuel pellet outside diameter,
- Fuel density,
- Fuel enrichment.

b) Uncertainties in boundary conditions:

- System pressure,
- System power,
- Coolant inlet temperature,
- Coolant flow rate.

The suggested range of uncertainty for those parameters are provided in the next two tables.

Table 1: Manufacturing Uncertainties

Parameter	Standard deviation
Cladding outside diameter	1.5%
Cladding thickness	1.5%
Cladding roughness	15%
Fuel pellet outside diameter	0.1%
Fuel density	0.5%
U^{235} enrichment	0.02%

Table 2: Core Boundary Condition Standard Deviations

Parameter	Standard deviation
System pressure	0.00333
Coolant flow rate	0.01667
System power	0.01667
Inlet fluid temperature	0.01

In the UAM Benchmark, modelling parameter uncertainties are left to the discretion of the participants except for the material property uncertainties which are handled separately. Suggested material property uncertainties are provided in the next table.

Funded by the European Union

Funded by the European Union. Views and opinions expressed are however those of the author(s) only and do not necessarily reflect those of the European Union or the European Atomic Energy Community ('EC-Euratom'). Neither the European Union nor the granting authority can be held responsible for them.

Table 3: Material properties recommended uncertainties

Parameter	Standard deviation
Fuel Thermal Conductivity	5%
Fuel Thermal Expansion	5%
Fuel Specific Heat	1.5%
Cladding Thermal Conductivity	5%
Cladding Thermal Expansion	5%

3.1.1.4 Preliminary assessment of the uncertainty

At this point, the uncertainty quantification is limited to the nuclear data uncertainty on the HELIOS model which is used for the cross-section generation. Once the coupled FENNECS/CTF model is better validated, the uncertainty quantification from all sources described above will be propagated through the coupled model. Moreover, the number of samples will be increased to allow a meaningful sensitivity analysis.

For this preliminary study, 100 samples were computed and analysed. The first QoI is the k_{eff} of the 2D core model. The obtained average of the k_{eff} is 1.12190. The uncertainty due to nuclear data uncertainty (i.e. standard deviation) is 517 pcm.

The second considered QoI is the multi-group flux in selected pins inside the core. The location of the selected pins is displayed in Figure 1.

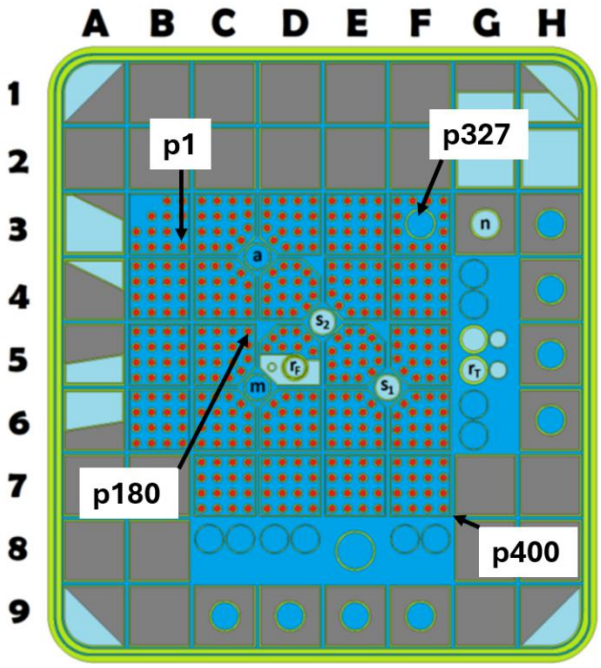


Figure 1: BME Training reactor core with position of analysed locations

Funded by the European Union

Funded by the European Union. Views and opinions expressed are however those of the author(s) only and do not necessarily reflect those of the European Union or the European Atomic Energy Community ('EC-Euratom'). Neither the European Union nor the granting authority can be held responsible for them.

Figure 2 shows a comparison of the average flux in the 7 energy groups for the 4 selected pins. The maximum flux is systematically found in energy group #7 (thermal). Pin#180, located toward the center of the core, has a higher flux level than all the other pins which are close to the reflector.

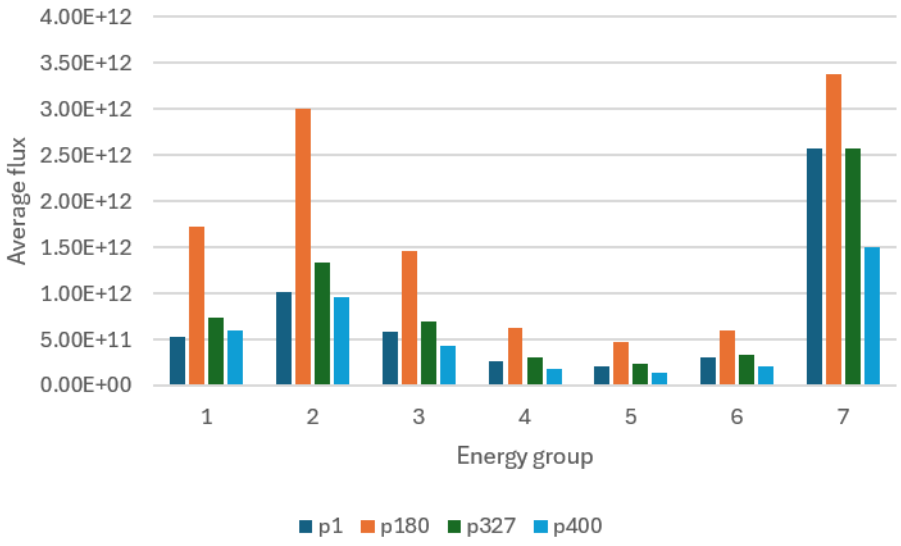


Figure 2: Average flux in the 7 energy groups for 4 selected pins.

Figure 3 shows the uncertainty (i.e. standard deviation) of the flux in each energy group. from the nuclear data. The uncertainty is almost completely independent on the pin location (i.e. flux level in the pin). The uncertainty is highest in energy group #1 (in which the neutrons are born), namely ca. 3%. It decreases to 1% in energy group #2. It is stable around 0.5% in energy groups #3 to #7.

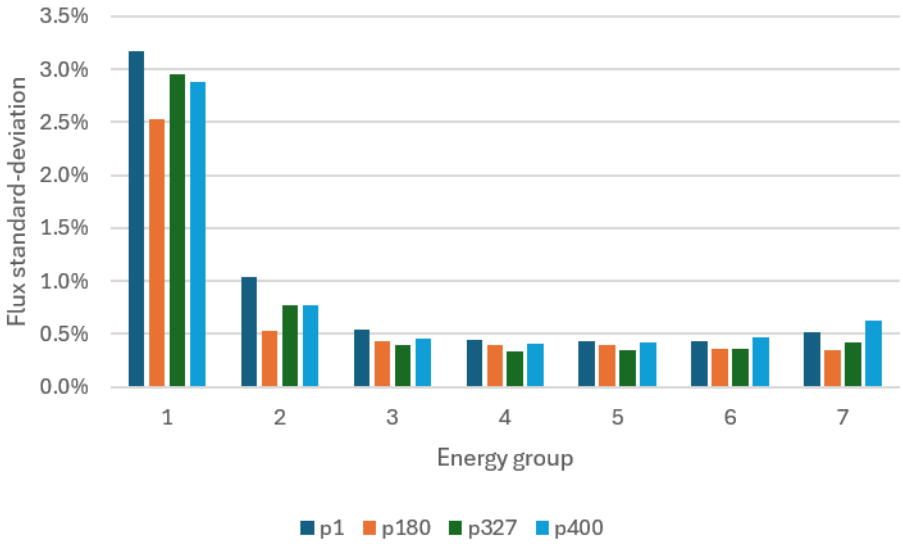


Figure 3: Standard deviation of the flux in 7 energy groups for 4 selected pins

3.1.2 EPFL Uncertainty Analysis

3.1.2.1 TRACE/PARCS model description

A brief description of the computational scheme used in this study is provided in this paragraph; a more complete description of the model can be found in D2.2 (Hursin et al., 2026). The coupled

Funded by the European Union

Funded by the European Union. Views and opinions expressed are however those of the author(s) only and do not necessarily reflect those of the European Union or the European Atomic Energy Community ('EC-Euratom'). Neither the European Union nor the granting authority can be held responsible for them.

calculation chain per sample relies on the conventional TRACE/PARCS model developed at BME(Vanyi, 2023). It proceeds as follows:

- 17 assemblies are modelled in Serpent2 (41 Serpent2 runs are required due to the various temperature and density branches), producing few-group cross-section libraries for the 300 random samples (17 PMAX files per sample);
- PARCS core calculations are run per sample: all-rods-out (ARO) and 2 control-rod-worth cases (automatic and manual bank), each in the “in” and “out” rod positions;
- 1 coupled TRACE/PARCS calculation is run per sample to model the FB#2 transient case.

This workflow is repeated for every random sample, building the ensembles from which the results of Section 3.1.2.4 are derived.

3.1.2.2 Nuclear data uncertainties

The nuclear data uncertainty is described by the ENDF/B-VII.1 covariance data, collapsed to a 19-energy-group structure. The perturbed isotopes and reaction channels are listed below.

- Isotopes: Pu-239, U-235, U-238, H-1, O-16, C-6, Ag-109, U-234, Pu-240, Mg-24, Mg-25
- Reaction channels: (n,el), (n,inel), (n,2n), (n,f), (n,γ), $\bar{\nu}$ (average number of neutrons per fission), χ (fission spectrum)

The isotope selection is composed of every isotope present in the nominal Serpent2 model of the BME reactor for which ENDF/B-VII.1 provides covariance information. Isotopes in the model without an associated covariance evaluation in ENDF/B-VII.1 are therefore not perturbed, and are implicitly treated as exactly known in this study.

3.1.2.3 Technological uncertainties

A set of technological and thermal-hydraulic input parameters relevant to the coupled TRACE/PARCS model of the BME reactor is perturbed. Table 4 lists the parameters and their assumed probability distributions.

Parameter	Distribution
Core inlet temperature (K)	U(296.6, 296.8)
Control rod position – in (mm)	N(380, 0.5)
Control rod position – out (mm)	N(420, 0.5)
Initial power (W)	N(1000, 10)
Isotopic composition multiplier	3% uncertainty (see text for details)
Heat transfer coefficient	N(1000, 10)
Friction factor multiplier	U(0.5, 1.5)
Hydraulic diameter multiplier	N(1, 5%)

Funded by the European Union

Funded by the European Union. Views and opinions expressed are however those of the author(s) only and do not necessarily reflect those of the European Union or the European Atomic Energy Community ('EC-Euratom'). Neither the European Union nor the granting authority can be held responsible for them.

Parameter	Distribution
Flow area multiplier	N(1, 5%)

Table 4: Technological and thermal-hydraulic uncertain input parameters and their assumed distributions.

In Table 1, the distributions are written in standard shorthand notation for probability distributions:

- U(a, b): a uniform distribution between the bounds *a* and *b*. For example, U(0.5, 1.5) for the friction factor multiplier means any value between 0.5 and 1.5 is drawn with equal probability.
- N(μ, σ): a Gaussian distribution with mean μ and standard deviation σ. For example, N(1000, 10) for the initial power means the sampled values are centered on 1000 W with a standard deviation of 10 W.

The heat transfer coefficient, friction factor, hydraulic diameter and flow area entries are straightforward multiplicative coefficients already exposed by the TRACE input (they scale, respectively, the wall/coolant heat-transfer correlation, the frictional pressure-drop correlation, the channel hydraulic diameter and the channel flow area used internally by TRACE). They are perturbed directly by sampling the multiplier itself from the distribution given in Table 4. These four distributions were derived from expert judgment to represent the upper bound of the actual uncertainty associated with the fuel or reactor geometry, or on the underlying heat-transfer/friction correlations themselves.

Unlike the four multipliers above, the isotopic-composition multiplier uncertainty was not assigned an arbitrary distribution directly on the fuel composition. Instead, it was derived from a dedicated set of BME fuel-pin depletion calculations in Serpent2, in which the target burnup of each sample is drawn from a normal distribution within 3% standard deviation of the representative fuel burnup for the BME reactor (0.8 MWd/kg), and propagated through depletion to obtain a corresponding ensemble of isotopic compositions. The actual calculation scheme comprises of four steps:

a. a set of Serpent2 fuel-pin depletion inputs is generated, one per sample, each with its own randomly sampled target burnup.

b. the Serpent2 depletion output of every sample is parsed to extract the atomic densities of the isotopes of interest (Np-237, Pu-239, Pu-240, U-234, U-235, U-236 and U-238) at the final step. The sample covariance of these isotopic concentrations across the ensemble is then computed, giving a composition covariance matrix shown in Figure 4.

c. Then, a correlated set of multiplicative isotope density factors is drawn from a multivariate normal distribution and applied to every occurrence of the corresponding isotope's atom density in the Serpent2 lattice input files, so that the isotope-to-isotope correlations captured by the depletion-based covariance matrix are preserved in the perturbed lattice compositions.

d. The perturbed Serpent2 lattice results for each sample are passed through GENPMAXS to generate the corresponding two-group PARCS cross-section libraries, and TRACE/PARCS core calculations are run producing the per-sample statistics used in the UQ study.

Funded by the European Union

Funded by the European Union. Views and opinions expressed are however those of the author(s) only and do not necessarily reflect those of the European Union or the European Atomic Energy Community ('EC-Euratom'). Neither the European Union nor the granting authority can be held responsible for them.

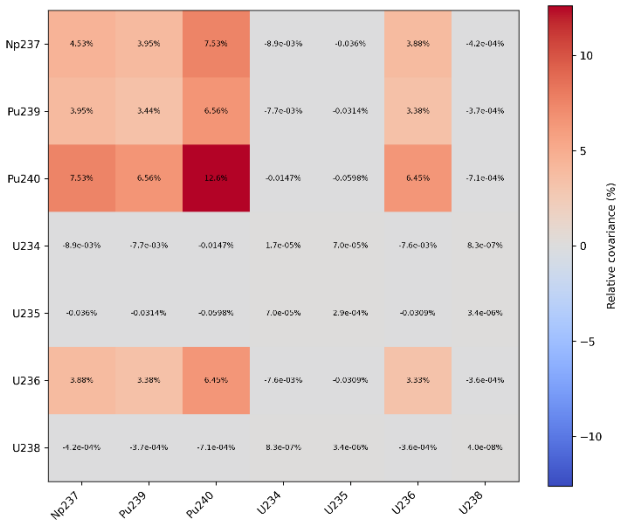


Figure 4: Relative covariance matrix (%) of the fuel isotopic composition.

The fuel composition covariance matrix shown in Figure 4 suggests two distinct groups of behaviour. Np-237, Pu-239, Pu-240 and U-236 (minor actinides produced during the depletion of the fuel) display large relative variances and are almost perfectly positively correlated with one another: since the target burnup is the only random variable sampled, and due to its small magnitude, every isotope rises and falls together from one sample to the next. By contrast, U-234, U-235 and U-238, whose inventories are dominated by the initial fuel loading, show small relative variances and negligible correlations. Such behaviour was expected due to the small value of fuel exposure.

3.1.2.4 Preliminary assessment of the uncertainty

This section presents the preliminary UQ and SA results obtained for the BME reactor FB#2 transient benchmark.

Quantities of interest

The following quantities of interest (QoIs) are considered:

- the steady-state core multiplication factor k_{eff}, evaluated for several control-rod configurations (all-rods-out; automatic bank in/out; manual bank in/out);
- the associated control-rod worths (derived from the AUT and MAN in/out k_{eff} pairs);
- the FB#2 transient reactor power trace, as computed by TRACE/PARCS;
- the FB#2 transient fuel/coolant temperature trace at instrumented location C7.

Reactivity uncertainties

Table 2 summarizes the mean keff and its standard deviation, in pcm, for each configuration, over the sampled ND perturbations.

Configuration	Mean keff	σ (pcm)
ARO	0.98577	1665
AUT out	0.98662	1667

Funded by the European Union

Funded by the European Union. Views and opinions expressed are however those of the author(s) only and do not necessarily reflect those of the European Union or the European Atomic Energy Community ('EC-Euratom'). Neither the European Union nor the granting authority can be held responsible for them.

Configuration	Mean keff	σ (pcm)
AUT in	0.98103	1656
MAN out	0.98754	1669
MAN in	0.97446	1643

Table 5: Mean keff and its standard deviation (in pcm) for the BME reactor configurations.

The propagated k_{eff} uncertainty is considerably larger than found in earlier studies with ENDF/B-VII.1; the sensitivity ranking below points to the U-235 $\bar{\nu}$ and χ covariances as the dominant contributors.

The running mean of the AUT and MAN rod worths (Figure 5) shows a brief transient over the first 10 to 20 samples, before settling into an essentially flat trend from roughly 100 samples onward. Beyond this point, extending the ensemble from 100 to 300 samples only introduces sub-pcm fluctuations around the converged value and does not change the estimated mean in any way that matters practically: 100 samples appear to be enough to estimate the computational uncertainty in this case.

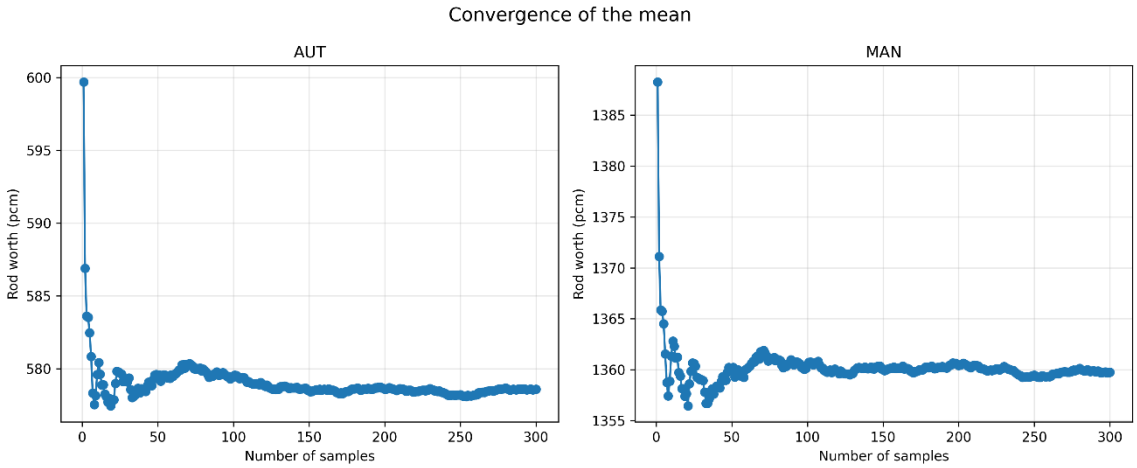


Figure 5: Convergence of the mean rod worth for the MAN and AUT control rods.

For the sake of completeness, the corresponding histograms (Figure 6), built from the full 300-sample ensemble, are shown in Figure 6. They appear essentially Gaussian, hinting that the relationship between input and output is linear. This is important for the sensitivity analysis that relies on a linearity assumption.

Funded by the European Union

Funded by the European Union. Views and opinions expressed are however those of the author(s) only and do not necessarily reflect those of the European Union or the European Atomic Energy Community ('EC-Euratom'). Neither the European Union nor the granting authority can be held responsible for them.

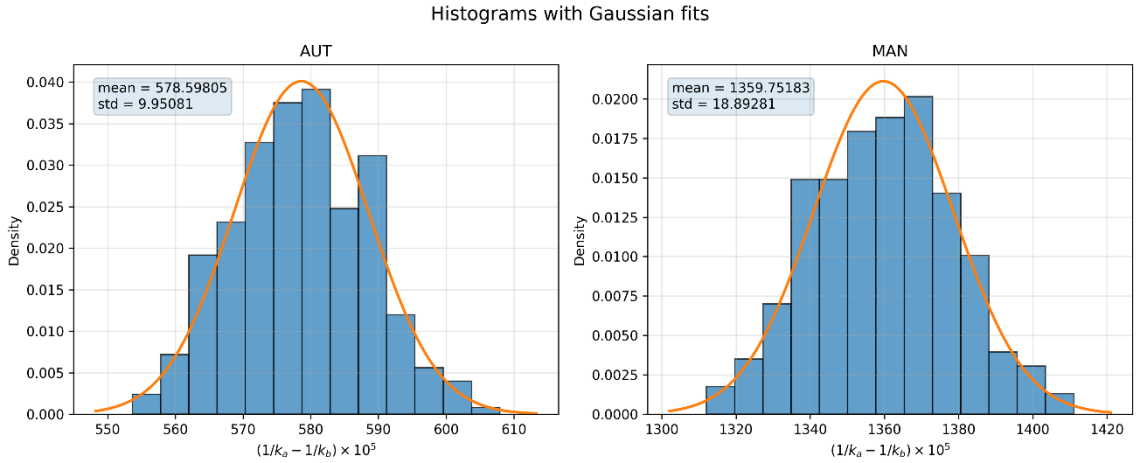


Figure 6: Distribution of rod worth samples.

Assuming a delayed neutron fraction of 654 pcm, the corresponding rod worth are shown in Table 6. The mean values obtained here are consistent with the values reported in (Vanyi, 2023): although the present model predicts somewhat larger absolute rod worths than the measurement and the earlier Serpent2/PARCS calculations (difference attributed to a slightly different cross-section generation in Serpent), the relative worth of the two banks is well reproduced. More importantly for the present UQ study, the propagated computational uncertainty on the rod worths is of the same order of magnitude as the experimental measurement uncertainty reported in the same thesis: the nuclear-data uncertainties propagated through the UQ workflow is not negligible compared to what is achievable experimentally.

	Δρ (¢)	σ(¢)
AUT	88.26	0.90
MAN	207.46	1.58

Table 6: Mean rod worth and its standard deviation (in $) for the BME reactor configurations.

As described above, the few-group cross-section libraries used by PARCS are generated from Serpent2, which means the cross sections themselves carry a purely statistical uncertainty inherited from the underlying Monte Carlo method. This source of noise is distinct from propagated input uncertainties (e.g., nuclear data covariances) and reflects the finite number of neutron histories used in the Serpent runs. Its impact on downstream PARCS results can be estimated by generating a small batch of repeated Serpent calculations (on the order of 100 samples) using the same nominal ACE cross-section files but different random number seeds, then propagating each resulting few-group library through PARCS. The spread in the resulting PARCS outputs quantifies the contribution of this Monte Carlo statistical noise to the overall computational uncertainty, independent of any physical nuclear data uncertainty. The purely statistical uncertainty on PARCS results is approximately 8 pcm on k_{eff} and 3 pcm (0.4 cts) on rod worths. Considering the results shown in Table 5 and Table 6, one can conclude that the Monte Carlo uncertainty is negligible for these quantities.

Finally, the isotopic-composition (burnup) uncertainty alone contributes approximately 30 pcm to the k_{eff} uncertainty and is negligible compared to the ND uncertainty.

Funded by the European Union

Funded by the European Union. Views and opinions expressed are however those of the author(s) only and do not necessarily reflect those of the European Union or the European Atomic Energy Community ('EC-Euratom'). Neither the European Union nor the granting authority can be held responsible for them.

Sensitivity analysis of k_{eff} (ARO configuration)

The regression-based sensitivity indices, obtained with the method described in Section 2.2.3, were computed for the ARO k_{eff} with respect to each of the sampled isotope-reaction pairs. Ranked by decreasing mean sensitivity index, the results are shown in Figure 7.

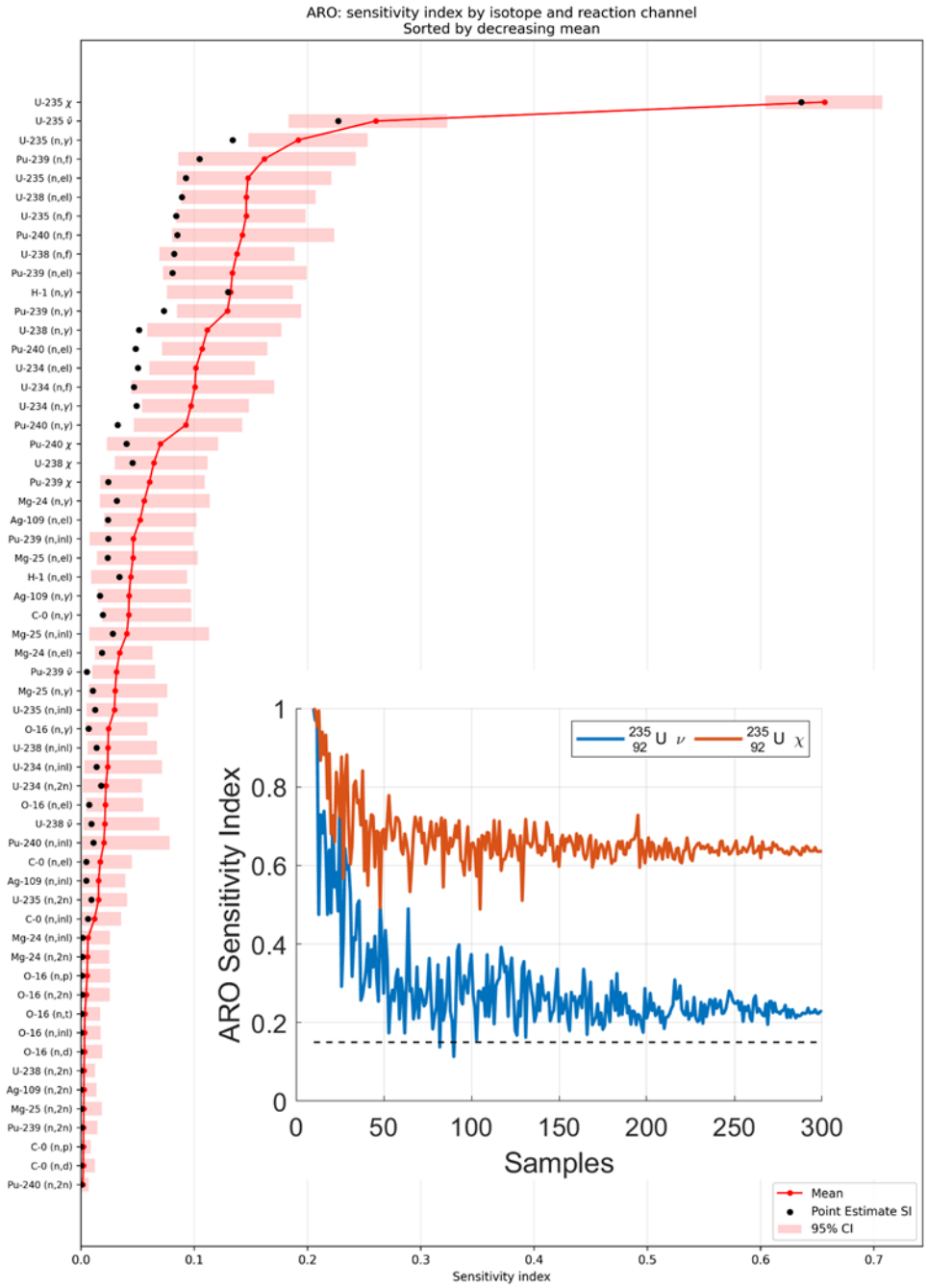


Figure 7: Contributor to the ARO keff uncertainty, ranked by GRS sensitivity index The convergence with the number of samples is also represented.

The two largest contributors are U-235 χ and U-235 ν̄. The convergence of the two leading sensitivity indices with the number of samples, also visible in Figure 7, shows U-235 χ stabilizing around a sensitivity index of 0.65 and U-235 ν̄ around 0.25 after about 100 samples are used, confirming that these two data are, by a clear margin, the dominant contributors to the k_{eff} uncertainty for this model. All other isotope-reaction pairs contribute sensitivity indices well below 0.2 which may not be

Funded by the European Union

Funded by the European Union. Views and opinions expressed are however those of the author(s) only and do not necessarily reflect those of the European Union or the European Atomic Energy Community ('EC-Euratom'). Neither the European Union nor the granting authority can be held responsible for them.

statistically significant given the number of samples. U-235 χ as leading term to the uncertainty is surprising (for LWR, U-235 ν̄ is usually the driver to the ND uncertainties with ENDF/B-VII.1 as reported in (Bratton et al., 2014)) and can probably be traced back to the higher enrichment of the EK-10 fuel of BME.

Transient (FB#2) power uncertainties

The TRACE-computed mean power trace for the FB#2 transient and the various samples are shown in Figure 8. The mean power trace reproduces the general shape of the corrected measured power reasonably well, though the range of possible values depicted by the spread of the various samples does not encompass the measurement data, early in the transient (between 700 and 1300s), showing that the model is biased and that a source of computational uncertainties has either not been considered or mis estimated.

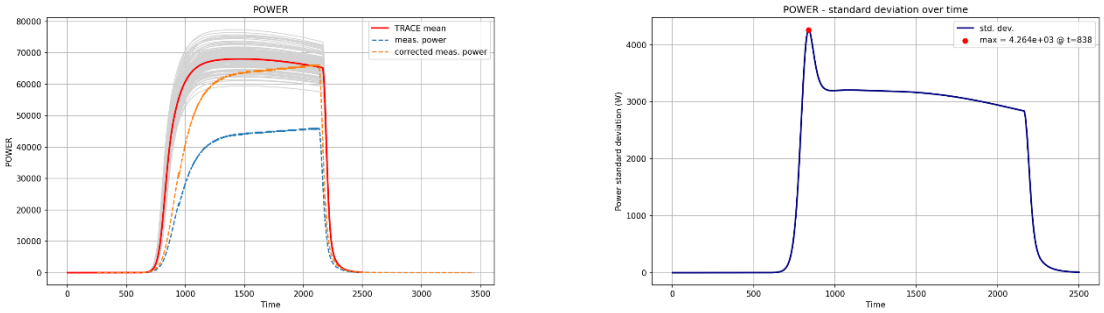
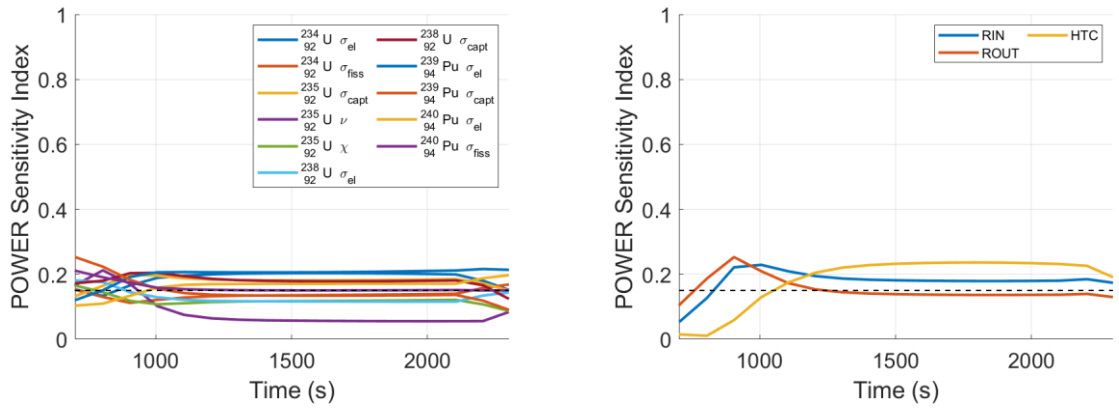


Figure 8: Evolution of the power computational uncertainty with time during the FB#2 transient.

The corresponding sensitivity analysis is shown in Figure 9. Sensitivity indices are computed at each time step of the transient. For the nuclear data inputs, the sensitivity indices of the leading isotope-reaction pairs (U-234, U-235, U-238, Pu-239 and Pu-240 elastic, capture and fission cross sections) are comparable in magnitude, roughly in the 0.1–0.25 range, indicating that the transient power response has no single dominant nuclear-data contributor; for the technological/TH inputs ("TH"), the initial position of the control rod tip and the heat-transfer coefficient are the leading contributors, with sensitivity indices peaking around 0.2–0.25 near the start of the power rise before settling to roughly 0.15–0.2 for the remainder of the transient.



a) Nuclear data b) technological parameters

Figure 9: Main contributors to the power uncertainty during the FB#2 transient.

Funded by the European Union

Funded by the European Union. Views and opinions expressed are however those of the author(s) only and do not necessarily reflect those of the European Union or the European Atomic Energy Community ('EC-Euratom'). Neither the European Union nor the granting authority can be held responsible for them.

Transient (FB#2) temperature uncertainties (channel C7)

The TRACE mean temperature trace at instrumented location C7 follows the general trend of the measured signal, although the measurement itself exhibits large fluctuations that are expectedly not reproduced by the calculated ensemble spread. It suggests some issues with the instrumentation.

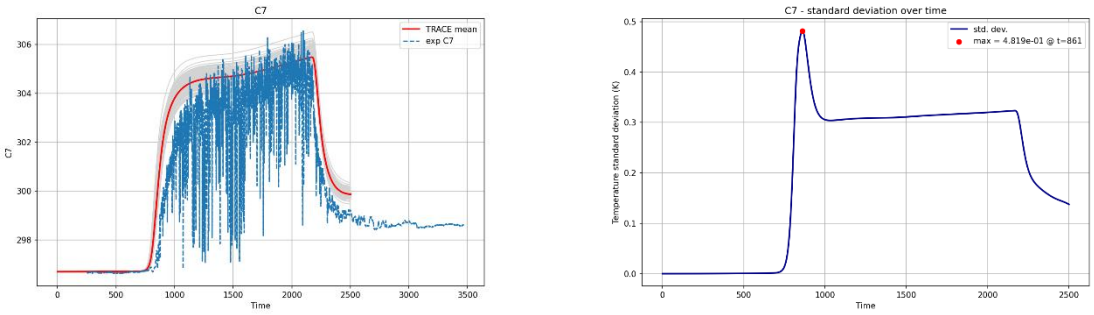
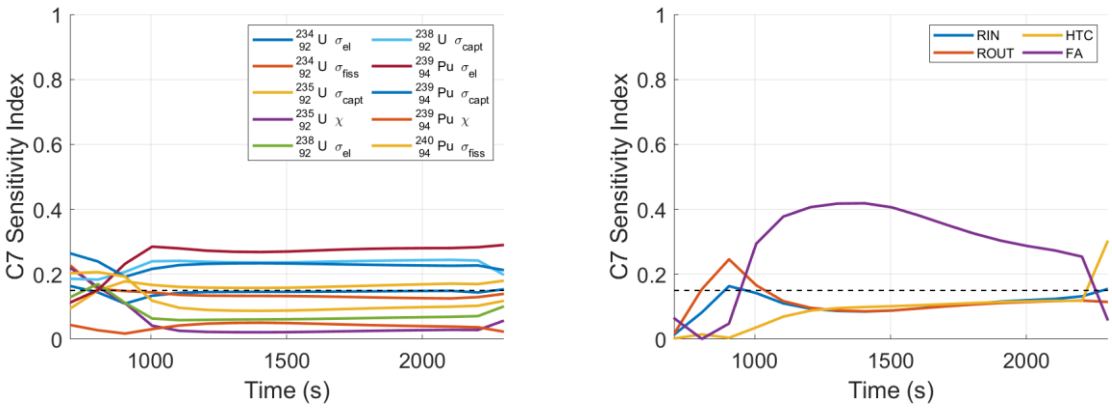


Figure 10: Evolution of the temperature computational uncertainty at the exit of the C7 channel, with time during the FB#2 transient.

The corresponding sensitivity analysis is shown in Figure 11. Sensitivity indices are computed at each time step of the transient. For the nuclear data inputs, the sensitivity indices are of a similar magnitude and spread to those found for the power earlier (roughly 0.05–0.25), with the U-238 capture cross section appearing as a comparatively larger contributor to the C7 temperature than to the power response. For the technological inputs, the flow-area multiplier (FA) becomes the dominant contributor to the C7 temperature uncertainty, with its sensitivity index rising to a peak of 0.4 around the middle of the transient markedly larger than the control-rod tip positions before and after movement (RIN, ROUT) or the heat-transfer coefficient (HTC), which remain in the 0.1 to 0.3 range throughout.



a) Nuclear data b) Technological parameters

Figure 11: Main contributors to the temperature uncertainty at the exit of the C7 channel, during the FB#2 transient.

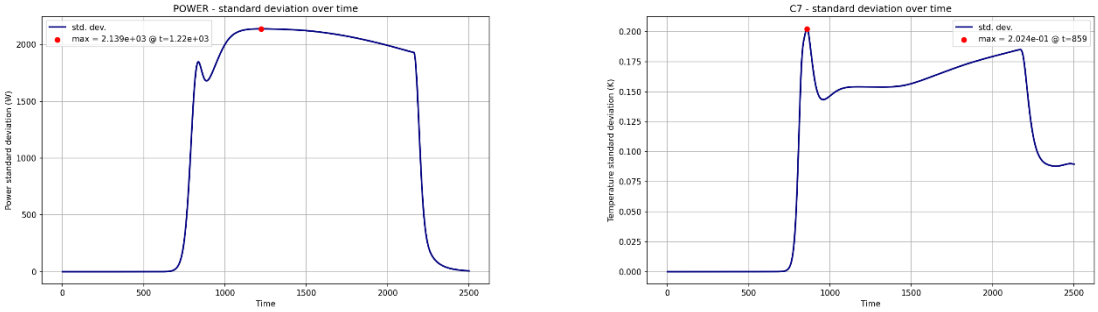
This contrasts with the power, for which the rod position and heat-transfer coefficient were the leading contributors to the technological uncertainties. The coolant flow area plays a larger role for the temperature response.

For the sake of completeness, the effect of the stochastic uncertainties due to the cross sections generation process is reported in Figure 12a for the power and Figure 12b for the temperature. On both cases, the resulting computational standard deviations are a factor two smaller than the nuclear data and technological uncertainties reported earlier. In the future, it might be desirable to increase

Funded by the European Union

Funded by the European Union. Views and opinions expressed are however those of the author(s) only and do not necessarily reflect those of the European Union or the European Atomic Energy Community ('EC-Euratom'). Neither the European Union nor the granting authority can be held responsible for them.

the number of particles used in the macroscopic library generation step but this will come at a significant computational cost.



a) Power b) C7 temperature

Figure 12: Effect of the Monte Carlo uncertainties in the macroscopic library generation process, on the transient uncertainties.

3.2 Budapest Research Reactor

This section summarizes preliminary results of the UQ and SA analysis performed on the BRR reactor model. The work follows a similar UQ/SA approach than the one previously carried out for the BME reactor (Section 3.1.2). For the BRR, the propagation of uncertainties currently covers mainly nuclear data uncertainties as the model relies of the Serpent2 input developed in D2.2 (Hursin et al., 2026). Such choice is supported by the limited impact of temperature feedback reported in that document. Additionally, the impact of the dosimeter position at the measurement location is analysed.

3.2.1 Nuclear data uncertainties

The nuclear-data uncertainties propagated through the BRR model are based on ENDF/B-VII.1 covariance data, condensed to a 19-energy-group structure. Covariances are propagated for the following isotopes and reaction channels:

- Isotopes: Pu-239, U-235, U-238, H-1, O-16, Ag-109, U-234, Pu-240, Mg-24, Mg-25, Be-9
- Reaction channels: elastic scattering (n,el), inelastic scattering (n,inel), (n,2n), fission (n,f), radiative capture (n,g), the average number of neutrons per fission (ν), and the fission spectrum (χ)

IRDFF-II dosimetry cross sections were additionally perturbed, using files generated with the SANDY code(Fiorito et al., 2017) to estimate the uncertainty in dosimeter response (see Section 3.2.3.6).

3.2.2 UQ/SA Methodology

Uncertainties are propagated using a simple random sampling approach:

- Random, correlated perturbations of the ENDF/B-VII.1 nuclear-data covariances are generated as randomly sampled ACE files using the NUSS tool.
- 300 perturbed samples are propagated through Serpent2 Monte Carlo transport calculations only.
- Dosimetry reaction uncertainties are obtained by computing multiple detector response (one per perturbed IRDFF-II file) from a nominal Serpent2 transport calculation. The random IRDDF files were generated with the SANDY code as NUSS was not capable of handling

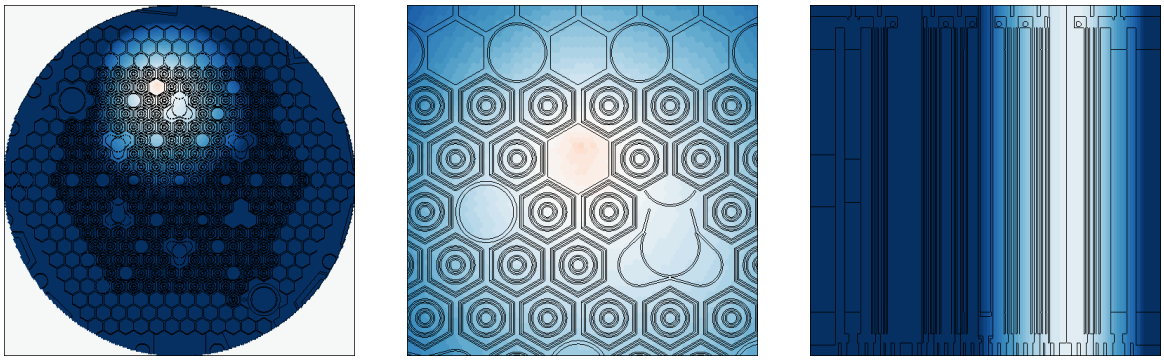
Funded by the European Union

Funded by the European Union. Views and opinions expressed are however those of the author(s) only and do not necessarily reflect those of the European Union or the European Atomic Energy Community ('EC-Euratom'). Neither the European Union nor the granting authority can be held responsible for them.

dosimetry cross sections. Some small modifications to the nominal SANDY workflow were still required.

To reduce the statistical (Monte Carlo) uncertainty in the region of the experimental setup in BRR, a variance-reduction scheme based on weight windows was set up following Serpent2's standard approach, targeting the fast-flux-trap location (the axial importance distribution assumed to be homogeneous in that region).

The importance maps resulting are shown in Figure 13 where one can distinctly see that the dosimetry measurement location carries a much larger importance (shades of red) than the other parts of the reactor (blue).



Radial view | Zoom in around the flux trap | Axial view

Figure 13: Importance map used during the fixed source Serpent2 calculations.

Prior to the ND propagation, a dedicated random-seed study was performed to characterize the purely statistical (Monte Carlo) contribution to the observed spread of results, independent of any nuclear-data perturbation. Its results are discussed in Section 3.2.3.2.

3.2.3 Results

3.2.3.1 Quantities of Interest

This section focuses on k_{eff}, the 2D (radial) assembly power distributions, as well as the axial profiles, at the fast-flux-trap location, of Au-197 (n,g), Fe-58 (n,g), and Fe-54 (n,p) reaction rates.

3.2.3.2 Computational uncertainty due to Monte Carlo statistics

A random-seed study (100 samples using nominal, unperturbed ACE files, varying only the Monte Carlo random seed in Serpent 2) was used to quantify the purely statistical contribution to the spread of results. The results are shown in Table 7

Quantity of interest	MC-statistical spread (100 samples, nominal data)
k_{eff}	14 pcm
Au-197 (n,g)	12 %
Fe-58 (n,g)	4 %
Fe-54 (n,p)	5 %

Funded by the European Union

Funded by the European Union. Views and opinions expressed are however those of the author(s) only and do not necessarily reflect those of the European Union or the European Atomic Energy Community ('EC-Euratom'). Neither the European Union nor the granting authority can be held responsible for them.

Quantity of interest	MC-statistical spread (100 samples, nominal data)
2D total power	0.5 %

Table 7: Monte Carlo statistical spread, from the random-seed study (nominal nuclear data).

This spread is likely too large to reliably resolve ND effects on the dosimetry-reaction responses but it is considered acceptable for assessing k_{eff} and power-distribution uncertainties. For the purpose of estimating the dosimetry reaction uncertainty, a much more detailed nominal Serpent2 calculation was required (100 times the number of neutron histories) to reduce the stochastic uncertainty to the point where the dosimetry reaction uncertainties become significant. This aspect explains the different treatments chosen for the transport and dosimetry nuclear data reported in Section 3.2.1.

3.2.3.3 k_{eff} Uncertainty

Nuclear-data uncertainty propagation yields a k_{eff} uncertainty of 984 pcm for the BRR configuration studied, dominated by the U-235 nubar covariance as shown in Figure 14. The ND standard deviation is nearly two orders of magnitude larger than the Monte Carlo statistical uncertainty reported in Table 7, confirming that the observed k_{eff} spread is driven by nuclear-data uncertainty rather than Monte Carlo noise.

Funded by the European Union

Funded by the European Union. Views and opinions expressed are however those of the author(s) only and do not necessarily reflect those of the European Union or the European Atomic Energy Community ('EC-Euratom'). Neither the European Union nor the granting authority can be held responsible for them.

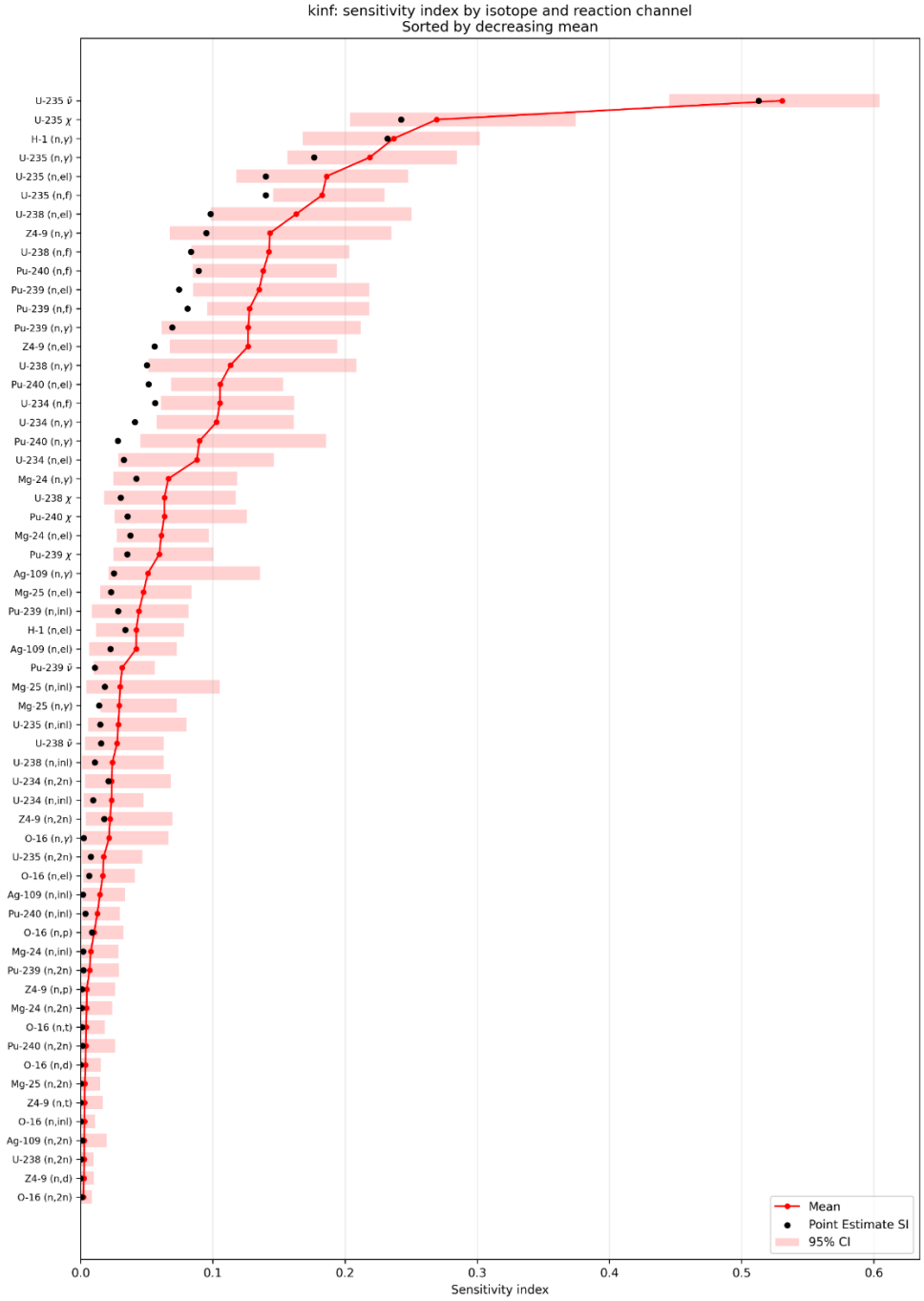


Figure 14: Nuclear-data-driven k_{eff} uncertainty for the sampled configurations.

3.2.3.4 2D Core Power Distribution

The power distribution uncertainties are shown in Figure 15. The 2D (radial) relative power uncertainty is below 0.5 % over most of the core, increasing toward the core periphery. Interestingly, the increase of relative standard deviation does not always happen in a low power region and as such suggests that an additional source of nuclear data uncertainty affects the power distribution in the core, possibly connected to the Beryllium reflector.

Funded by the European Union

Funded by the European Union. Views and opinions expressed are however those of the author(s) only and do not necessarily reflect those of the European Union or the European Atomic Energy Community ('EC-Euratom'). Neither the European Union nor the granting authority can be held responsible for them.

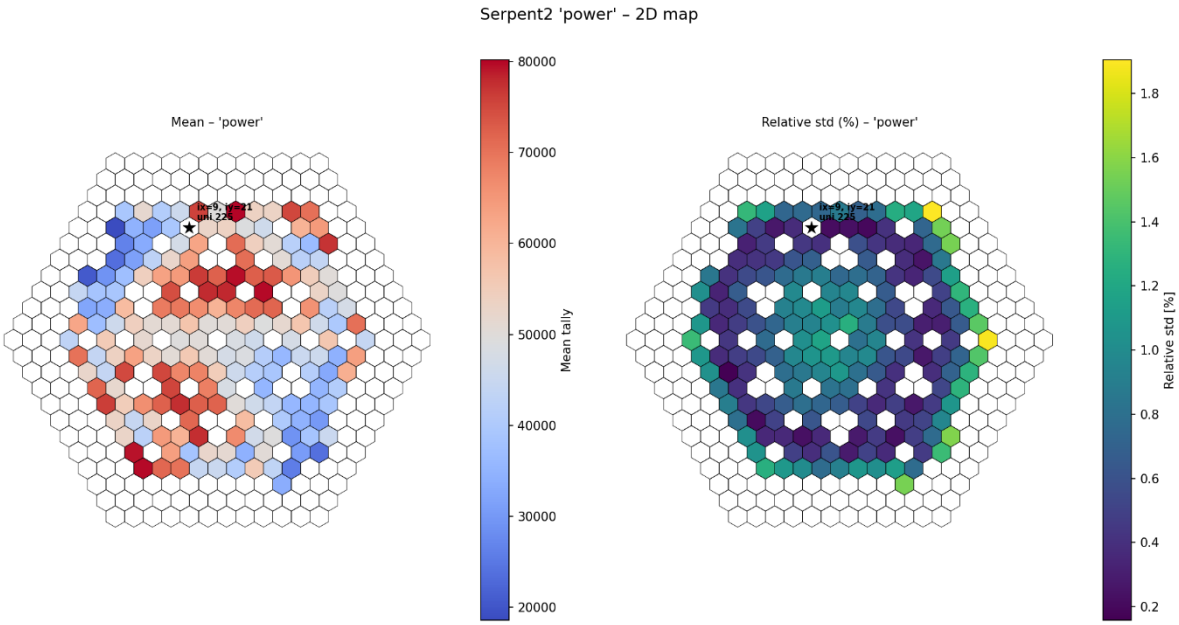


Figure 15: Mean and relative-standard-deviation maps for the 2D core power distribution.

3.2.3.5 Axial Dosimetry-Response and Flux Uncertainties at the Fast Flux Trap

Propagating the full set of 300 perturbed samples in the Serpent2 calculation of BBR allows to estimate the computational uncertainties due to nuclear data in the transport calculation on the reaction rates relevant for the dosimetry measurement. In this section, the IRDFF-2 nominal files are used and the uncertainties associated with those reactions are not considered. The resulting mean and spread of the three reaction rate profiles are shown in Figure 16 and Figure 17 for Au-197 (n,g) and Fe-58 (n,g) reaction rates respectively.

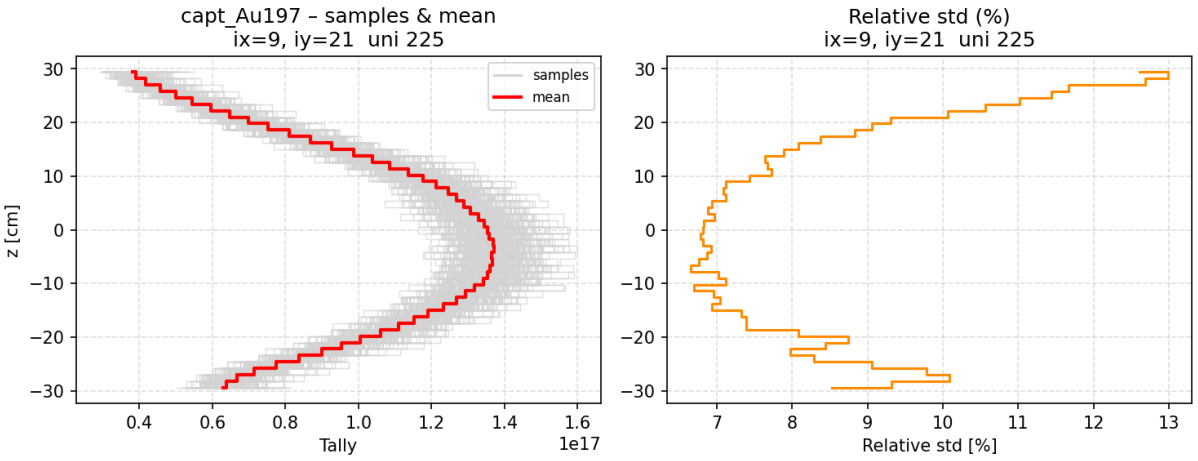


Figure 16: Axial variation and sensitivity indices for the Au-197 (n,g) response at the fast flux trap.

Funded by the European Union

Funded by the European Union. Views and opinions expressed are however those of the author(s) only and do not necessarily reflect those of the European Union or the European Atomic Energy Community ('EC-Euratom'). Neither the European Union nor the granting authority can be held responsible for them.

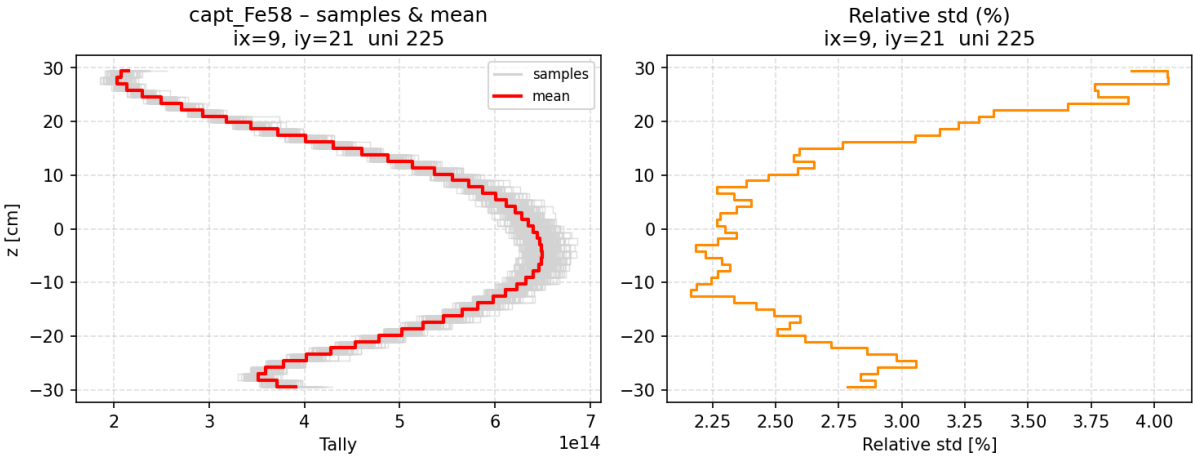


Figure 17: Axial variation and sensitivity indices for the Fe-58 (n,g) response at the fast flux trap.

For those quantities, the ND-propagated spread is comparable to the Monte Carlo statistical uncertainties reported in Section 3.2.3.2 demonstrating that these response fluctuations are driven mainly by Monte Carlo statistics. The Fe-54 (n,p) response is a notable exception: its relative standard deviation is shown in Figure 18.

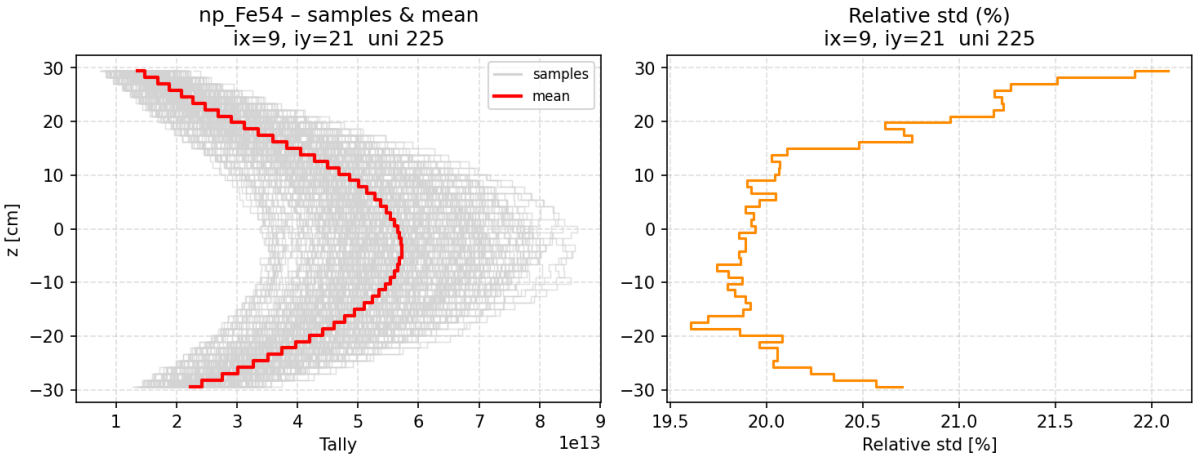


Figure 18: Axial variation for the Fe-54 (n,p) response at the fast flux trap.

It is much larger than the Monte Carlo uncertainties (20% vs 5 %), and sensitivity analysis (see Figure 19) identifies the U-235 fission-spectrum (χ) covariance as the dominant contributor, with a sensitivity index close to unity across the entire flux-trap region.

Funded by the European Union

Funded by the European Union. Views and opinions expressed are however those of the author(s) only and do not necessarily reflect those of the European Union or the European Atomic Energy Community ('EC-Euratom'). Neither the European Union nor the granting authority can be held responsible for them.

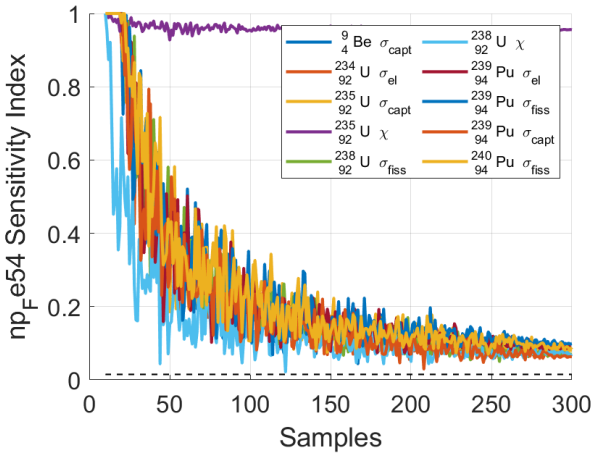


Figure 19: Sensitivity indices for the Fe-54 (n,p) response at the fast flux trap.

This large uncertainty is attributed to the Fe-54 (n,p) reaction threshold falling in an energy region where the U-235 fission-spectrum covariance is highly uncertain as depicted in Figure 20.

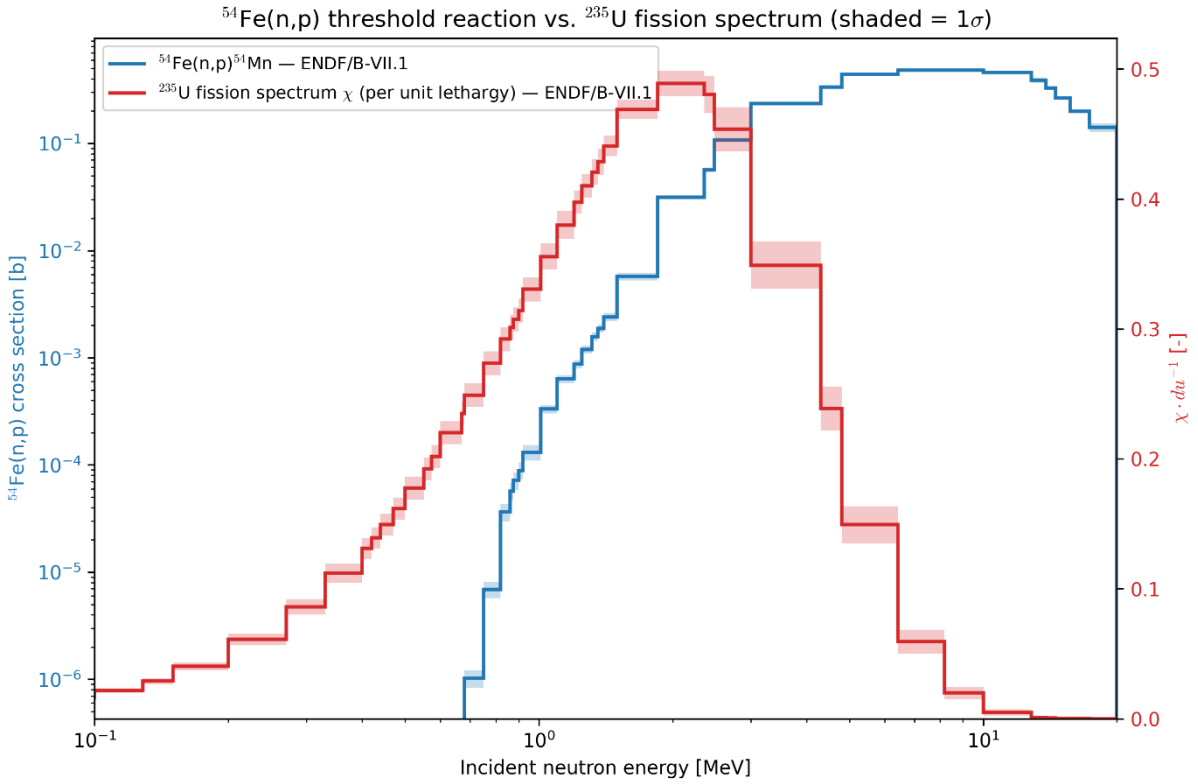


Figure 20: Fe-54 (n,p) threshold region overlaid on the U-235 fission-spectrum uncertainty, explaining the large propagated uncertainty.

3.2.3.6 Uncertainty Due to IRDFF Dosimetry Cross Sections

The contribution of IRDFF-II dosimetry cross-section uncertainty (as distinct from transport nuclear-data uncertainty) was evaluated from a single variance-reduced Serpent2 run using many more neutron histories and 100 dosimetry-ACE-file samples perturbed with SANDY. The range of computational uncertainties due solely to the dosimetry reactions are shown in Table 9 and illustrated in Figure 21.

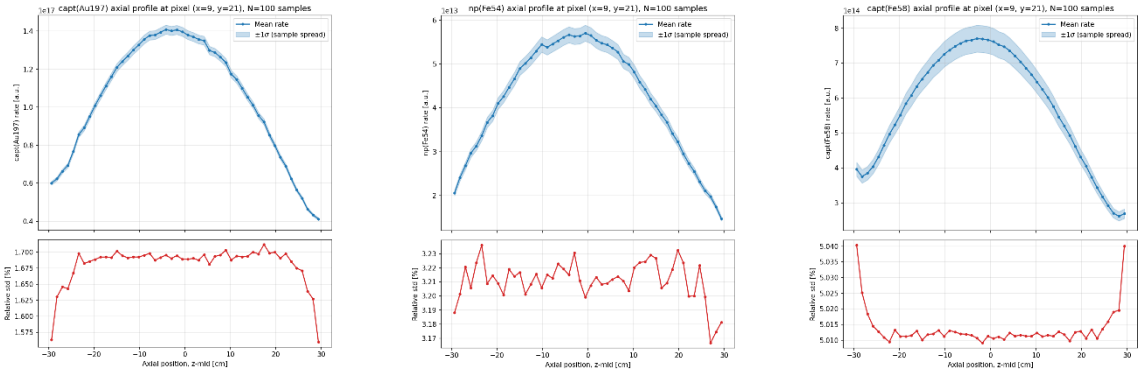
Funded by the European Union

Funded by the European Union. Views and opinions expressed are however those of the author(s) only and do not necessarily reflect those of the European Union or the European Atomic Energy Community ('EC-Euratom'). Neither the European Union nor the granting authority can be held responsible for them.

Reaction	Relative std. dev. (axial profile)
Au-197 (n,g)	1.57 % to 1.70 %
Fe-54 (n,p)	3.17 % to 3.23 %
Fe-58 (n,g)	5.01 % to 5.04 %

Table 8: Relative standard deviation attributable to IRDFF-II dosimetry cross-section uncertainty alone.

These uncertainties are negligible compared to the Monte Carlo statistics (Au-197 and Fe-54) or the nuclear data uncertainties (Fe-58). Their magnitude do not appear to significantly vary with the axial position of the dosimeter.



Au-197 (n,g) Fe-54 (n,p) Fe-58 (n,g)

Figure 21: Mean axial reaction-rate profiles (±1σ sample spread) and relative standard deviation, from IRDFF-II dosimetry cross-section perturbations.

3.2.3.7 Radial Variation at the Flux Trap

To estimate the uncertainty associated with the positioning of the dosimeter within the measurement location within the BRR flux trap, the radial (in-plane) variation of the three dosimeter reaction rates around the nominal detector position is assessed. Using a fine mesh tally for the three dosimetry reaction rates, the results shown in Figure 22 Figure 23 and Figure 24, were obtained, also with 100 times the number of neutron histories (as in Section 3.2.3.6). They represent the spread of tally values (mean and standard deviation) around the nominal detector position within the flux trap.

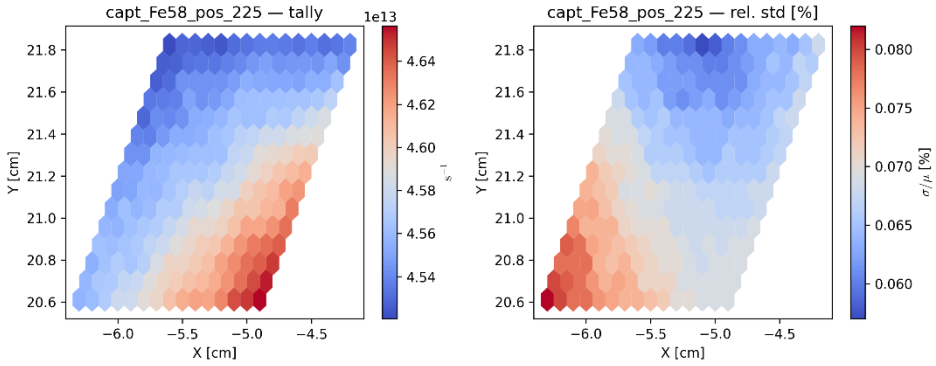


Figure 22: Mean and relative standard deviation of a mesh tally covering the flux-trap location for the Fe-58 (n,g) reaction rates.

Funded by the European Union

Funded by the European Union. Views and opinions expressed are however those of the author(s) only and do not necessarily reflect those of the European Union or the European Atomic Energy Community ('EC-Euratom'). Neither the European Union nor the granting authority can be held responsible for them.

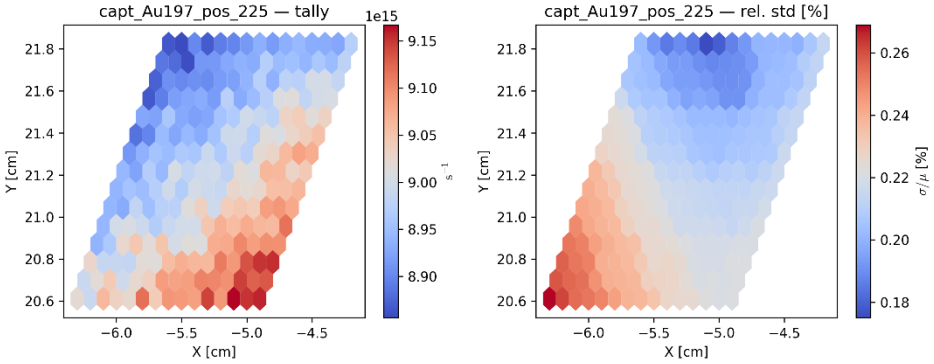


Figure 23: Mean and relative standard deviation of a mesh tally covering the flux-trap location for the Au-197 (n,g) reaction rates.

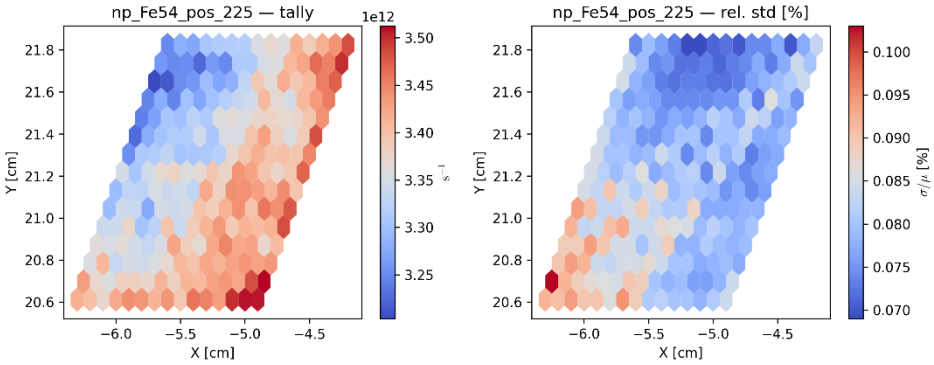


Figure 24: Mean and relative standard deviation of a mesh tally covering the flux-trap location for the Fe-54 (n,p) reaction rates.

A summary of the reaction rate distributions is provided in Table 9. The relative standard deviation of this radial spread is smaller than the IRDFF-2 uncertainty. This spread represents an upper bound on the positioning uncertainty of the reaction rate, and is largest for Fe-54 (n,p), at around 2 %. This indicates that an accurate control of the dosimeter placement within the flux trap is currently not required.

Dosimeter	Min	Max	Mean	Rel. Std. [%]
Au-197 (n,g)	8.86E+15	9.17E+15	9.00E+15	0.76
Fe-58 (n,g)	4.52E+13	4.66E+13	4.57E+13	0.68
Fe54 (n,p)	3.20E+12	3.51E+12	3.37E+12	1.90

Table 9: Radial spread of dosimetry reaction rates around the nominal position within the flux trap.

3.3 JSI TRIGA reactor

This section presents the uncertainty quantification analyses performed on the JSI Mark II TRIGA reactor model by two independent partners, GRS and JSI. Section 3.3.1 presents a summary of previous work carried out at JSI to quantify computational uncertainties. Section3.3.2 describes the GRS approach, which couples the neutronics code FENNECS with the thermal-hydraulics subchannel code

Funded by the European Union

Funded by the European Union. Views and opinions expressed are however those of the author(s) only and do not necessarily reflect those of the European Union or the European Atomic Energy Community ('EC-Euratom'). Neither the European Union nor the granting authority can be held responsible for them.

CTF in an open-core representation, focusing on thermal-hydraulics and nuclear data uncertainties following the UAM-LWR benchmark methodology.

3.3.1 JSI Uncertainty Analysis

This section provides a summary of uncertainties associated with modelling of the JSI TRIGA benchmark experiments described in the EVEREST D2.1 report (Czifrus et al., 2026). The modelling uncertainties differ by experiment but share common origins in Monte Carlo statistics, nuclear data or material composition, as well as geometric and physical simplifications. The various uncertainty magnitudes are summarized in Table 10 below, see (Czifrus et al., 2026), sections 5.3.1 to 5.3.5 for details.

For the Au-197 (n,g) axial profile measurements, Monte Carlo statistical uncertainty stays below 1% in the core mid-plane (rising to 2% near the grid plates), the choice of nuclear data library (ENDF/B-VII.1, ENDF/B-VII.0, ENDF/B-VI.6, JEFF-3.1) contributes only about 2%. The leading term for the uncertainty is the 5 to 10% uncertainty in the absolute power calibration.

For the axial fission-rate measurements with the U-235 and U-28 fission chambers, the combined modelling uncertainty (calibration, fuel composition, and MC statistics) totals between 2.6 and 4.0%, while fuel burn-up stands out as the largest systematic bias, shifting the response by +3.5 ± 2.0% (U-235) and +1.0 ± 0.5% (U-238) relative to a fresh-fuel model, well above the negligible contributions from geometry, impurities, control-rod position, and temperature effects.

For the reactor pool CFD simulations (steady-state and natural-convection transients), the leading modelling uncertainty is geometric: neglecting the 5 m control-rod guide tubes underestimates hydraulic resistance and vertical temperature gradients, while mesh refinement, turbulence-model choice, heat losses through the pool walls, and the idealized Heaviside power ramp-up are each secondary contributor.

Finally, for the in-core temperature-profile measurements at MP5, MP14, MP16, and MP21, the CFD model consistently and slightly underestimates measured coolant temperatures, with azimuthal mixing between fuel rods identified as an effect not yet fully captured by the model, motivating further sensitivity analysis of core inlet velocity.

Experiment	Uncertainty Source	Magnitude
Au-197 (n,g) axial profile	MC statistical uncertainty	<1% (mid-plane), <2% (near grid plates)
	Nuclear data library choice	~2% (library-to-library spread)
	Absolute power/scaling normalization	5 to 10%
Axial fission rate (U-235 / U-238 fission chambers)	FC calibration	2.2% (both)
	Fuel isotopic composition	1.4% (^{235}U), 1.6% (^{238}U)
	MC statistical uncertainty	0.4 to 3%

Funded by the European Union

Funded by the European Union. Views and opinions expressed are however those of the author(s) only and do not necessarily reflect those of the European Union or the European Atomic Energy Community ('EC-Euratom'). Neither the European Union nor the granting authority can be held responsible for them.

Experiment	Uncertainty Source	Magnitude
	Combined modelling uncertainty	2.6 to 4.0% (U-235), 2.7 to 4.0% (U-238)
	Fuel burn-up bias (vs. fresh fuel)	+3.5 ± 2.0% (U-235), +1.0 ± 0.5% (U-238)
Reactor pool CFD (with/without cooling)	Geometry simplification (control-rod guide tubes)	Underestimates hydraulic resistance if omitted
	Mesh resolution	<1°C between refinement levels
	Turbulence model (k-ε vs. SST)	Differences confined to region near core (A10)
	Heat losses through pool walls	Minor, more pronounced at pool edge
	Power ramp-up idealization	Affects mainly the early stage of the transient
In-core temperature (MP5, MP14, MP16, MP21)	General model bias	Slight underestimation of measured temperatures
	Azimuthal mixing / orientation effects	Not fully captured

Table 10: Summary of Modelling Uncertainties by Experiment

3.3.2 GRS Uncertainty Analysis

3.3.2.1 Model description

A brief description of the models is provided in this paragraph; a more complete description of the models and results can be found in D2.2 (Hursin et al., 2026).

The GRS model focuses on the core (open-core representation), wherein the neutronics code FENNECS is coupled with the thermal-hydraulics subchannel code CTF. The rest of the reactor pool is not modelled. Instead, the inlet massflow and temperatures are given as boundary conditions.

Cross-section libraries for the FENNECS code are generated using the Serpent model provided by JSI, which was modified to generate all the required cross-section libraries.

3.3.2.2 Nuclear data uncertainties

The isotope selection is composed of every isotope present in the nominal Serpent2 model of the JSI TRIGA reactor for which ENDF/B-VII.1 provides covariance information. Isotopes in the model without an associated covariance evaluation in ENDF/B-VII.1 are therefore not perturbed, and are implicitly treated as exactly known in this study.

Funded by the European Union

Funded by the European Union. Views and opinions expressed are however those of the author(s) only and do not necessarily reflect those of the European Union or the European Atomic Energy Community ('EC-Euratom'). Neither the European Union nor the granting authority can be held responsible for them.

3.3.2.3 Other sources of uncertainty

The experience from the Uncertainty (UAM-LWR) benchmark from the OECD/NEA (Bratton et al., 2014) is used as basis for selecting the uncertain parameters as well as their uncertainty range. Various sources of uncertainties are examined such as modelling uncertainties, boundary condition uncertainties, and geometry/manufacturing uncertainties.

Unlike for the BME Training Reactor which uses fuel bundles containing relatively standard fuel pins (with a fuel pellet surrounded by cladding), several manufacturing tolerances are not applicable to the TRIGA reactor.

The suggested range of uncertainty for those parameters are provided in the next two tables.

Table 11: Manufacturing Uncertainties

Parameter	Standard deviation
Fuel outside diameter	1.5%
Fuel outside roughness	15%
Fuel density	0.5%
U^{235} enrichment	0.02%

Table 12: Core Boundary Condition Standard Deviations

Parameter	Standard deviation
System pressure	0.00333
Coolant flow rate	0.01667
System power	0.01667
Inlet fluid temperature	0.01

In the UAM Benchmark, modelling parameter uncertainties are left to the discretion of the participants except for the material property uncertainties which are handled separately. Suggested material property uncertainties are provided in the next table.

Table 13: Material properties recommended uncertainties

Parameter	Standard deviation
Fuel Thermal Conductivity	5%
Fuel Thermal Expansion	5%

Funded by the European Union

Funded by the European Union. Views and opinions expressed are however those of the author(s) only and do not necessarily reflect those of the European Union or the European Atomic Energy Community ('EC-Euratom'). Neither the European Union nor the granting authority can be held responsible for them.

Parameter	Standard deviation
Fuel Specific Heat	1.5%
Cladding Thermal Conductivity	5%
Cladding Thermal Expansion	5%

3.3.2.4 Preliminary assessment of the uncertainty

At this point, the uncertainty quantification is limited to the nuclear data uncertainty on the Serpent 2 model which is used for the cross-section generation. Once the coupled FENNECS/CTF model is better validated, the uncertainty quantification from all sources described above will be propagated through the coupled model. Moreover, the number of samples will be increased to allow a meaningful sensitivity analysis.

For this preliminary study, 100 samples were computed and analysed. The first QoI is the k_{eff} of the 3D reactor model. The obtained average k_{eff} is 1.10806. The uncertainty caused by the nuclear data (i.e. the standard deviation) is 865 pcm which is to be compared to the average of the stochastic uncertainty 12 pcm.

The second considered QoI is the multi-group flux in selected pins inside the core. The location of the selected pins is displayed in Figure 25.

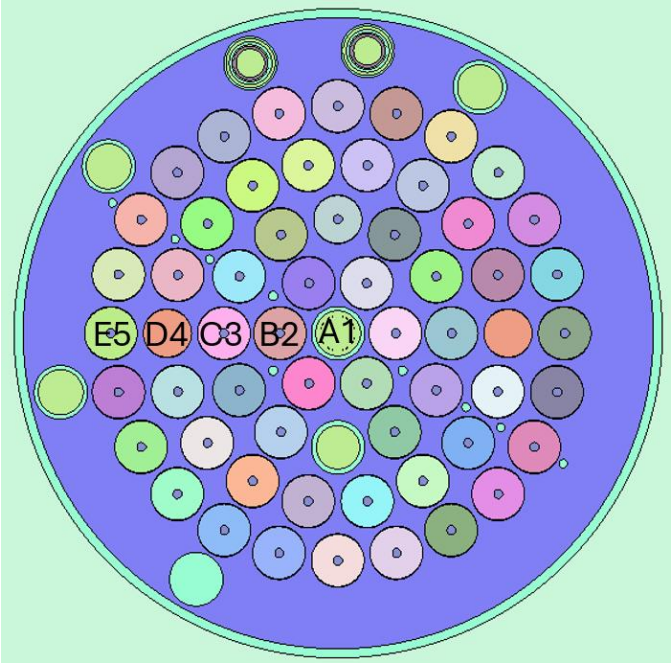


Figure 25: JSI TRIGA core with position of analysed locations

Figure 26 shows the average flux in the 2 energy groups for the 5 selected pins A1, B2, C3, D4 and E5. The maximum value is found in the central pin A1. It decreases as the pins get further from the core. The flux is larger in the fast group #1.

Funded by the European Union

Funded by the European Union. Views and opinions expressed are however those of the author(s) only and do not necessarily reflect those of the European Union or the European Atomic Energy Community ('EC-Euratom'). Neither the European Union nor the granting authority can be held responsible for them.

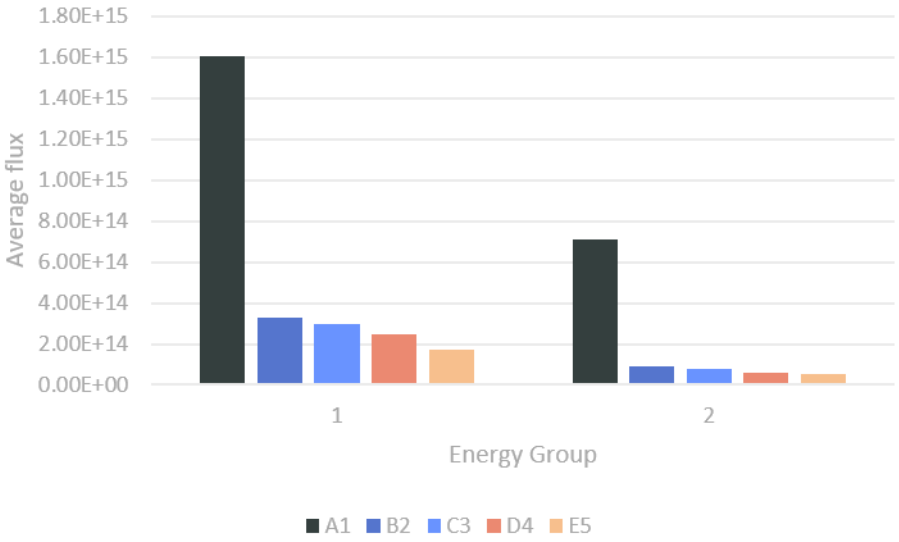


Figure 26: Average flux in the 2 energy groups for 5 selected pins

Figure 27 shows the uncertainty caused by the nuclear data as the relative standard deviation. In the fast group #1, it is constant at 1%. In the thermal group #2, it is 2.23% in A1 and decreases as the pin get further from the center of the core: only 1.29% in E5. However, it is important to put this result in perspective by looking at the average stochastic uncertainty (see Figure 28). As expected, the stochastic uncertainty increases continuously from A1 (0.30% in group #2) to E5 (0.54% in group #2): in E5 the stochastic can no longer be neglected in front of the nuclear data uncertainty. In further analyses, the statistics of the Monte Carlo simulation will be improved in order to minimize this effect.

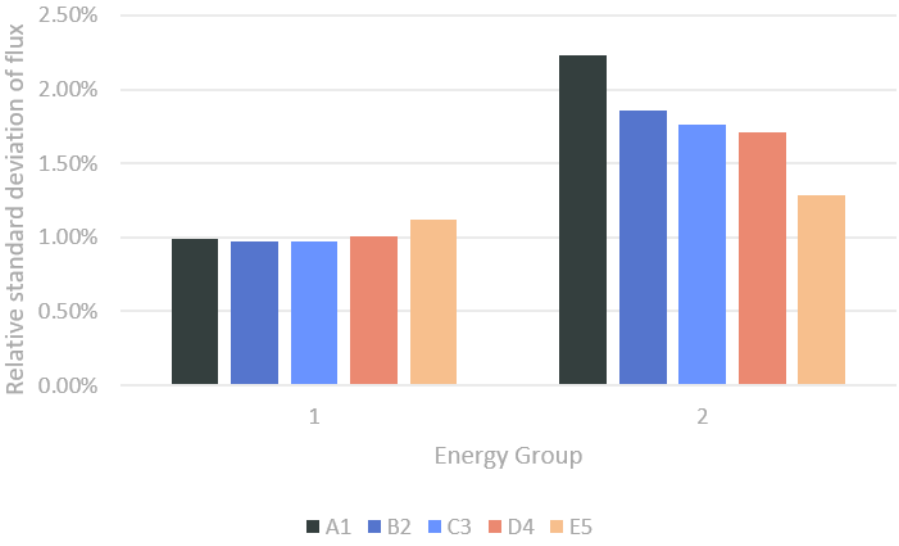


Figure 27: Relative standard deviation of the flux in 2 energy groups for 5 selected pins

Funded by the European Union

Funded by the European Union. Views and opinions expressed are however those of the author(s) only and do not necessarily reflect those of the European Union or the European Atomic Energy Community ('EC-Euratom'). Neither the European Union nor the granting authority can be held responsible for them.

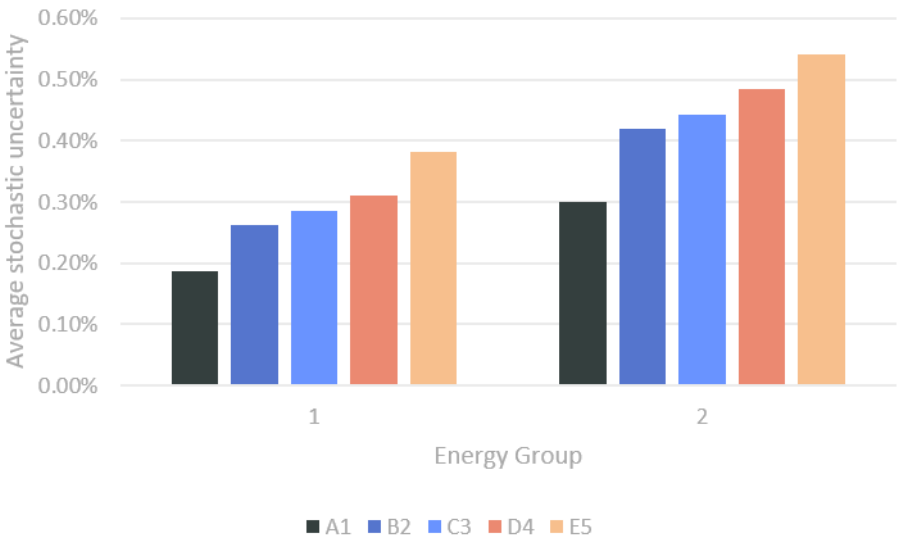


Figure 28: Average stochastic uncertainty of the flux in 2 energy groups for 5 selected pins

Funded by the European Union

Funded by the European Union. Views and opinions expressed are however those of the author(s) only and do not necessarily reflect those of the European Union or the European Atomic Energy Community ('EC-Euratom'). Neither the European Union nor the granting authority can be held responsible for them.

4 Conclusions and further work

Uncertainty quantification frameworks have been set up at GRS and EPFL for each of the three research reactors within the consortium: the Budapest Research Reactor, the BME Training Reactor, and the JSI TRIGA Mark II reactor. Both GRS and EPFL apply random sampling-based approaches.

For the BME TR, the GRS approach, which couples the neutronics code FENNECS with the thermal-hydraulics subchannel code CTF in an open-core representation, focuses on thermal-hydraulics and nuclear data uncertainties following the UAM-LWR benchmark methodology. At this point, the uncertainty quantification is limited to the nuclear data uncertainty on the HELIOS model which is used for the cross-section generation. For this preliminary study, 100 samples are computed and analysed.

In the EPFL approach, based on the Serpent2/TRACE/PARCS calculation scheme, nuclear data uncertainties and technological parameters uncertainties are propagated through a 300-sample ensemble to assess the steady-state reactivity, control-rod worths, and the FB#2 transient response

For the BRR, the propagation of uncertainties currently covers mainly nuclear data uncertainties as the model relies of the Serpent2 input developed in D2.2. Such choice is supported by the limited impact of temperature feedback reported in that document.

For the JSI TRIGA reactor, the GRS approach is the same as for the BME pipeline except for the cross-section generation tool which is switched from HELIOS to Serpent 2. At this point, the uncertainty quantification is limited to the nuclear data uncertainty on the Serpent 2 model which is used for the cross-section generation. For this preliminary study, 100 samples were computed and analysed. In some cases, the stochastic uncertainty can no longer be neglected in front of the nuclear data uncertainty. In further analyses, the statistics of the Monte Carlo simulation will be improved in order to minimize this effect.

In addition, a summary of previous work carried out at JSI to quantify computational uncertainties is presented.

Further work

Further work on the GRS side will be performed once the coupled FENNECS/CTF models for the BME TR and the JSI TRIGA reactor is better validated, the uncertainty quantification from all sources described above will be propagated through the coupled model. Moreover, the number of samples will be increased to allow a meaningful sensitivity analysis.

It is important to note that the list of uncertainty parameters and their associated uncertainty distribution are not set in stone. Indeed some parameters and values for the uncertainty range may be changed in the future to converge together with the EPFL team on a set of consistent values.

Funded by the European Union

Funded by the European Union. Views and opinions expressed are however those of the author(s) only and do not necessarily reflect those of the European Union or the European Atomic Energy Community ('EC-Euratom'). Neither the European Union nor the granting authority can be held responsible for them.

Bibliography

Aures, A., Eisenstecken, T., Elts, E., & Kilger, R. (2025). Nuclear data uncertainty propagation in continuous-energy Monte Carlo calculations. *Annals of Nuclear Energy*, *211*. https://doi.org/10.1016/j.anucene.2024.110955

Bousquet, J., Stoll, U., Velkov, K., Zwermann, W., Wemple, C., & Simeonov, T. (2018). Nuclear Data Uncertainty Propagation with HELIOS2 and XSUSA for LWR Systems. *Proceedings of PHYSOR 2018*.

Bratton, R. N., Avramova, M., & Ivanov, K. (2014). Oecd/nea benchmark for uncertainty analysis in modeling (UAM) for LWRS - summary and discussion of neutronics cases (PHASE I). *Nuclear Engineering and Technology*, *46*(3), 313–342. https://doi.org/10.5516/NET.01.2014.710

Czifrus, S., Perin, Y., Hursin, M., Vanyi, A., Ambrožič, K., & Belgya, T. (2026). D2 . 1 - Report describing the experiments performed at each reactor and associated data uncertainties. *EVEREST Delivrable*, *2.1*, 1–100.

Fiorito, L., Zerovnik, G., Stankovskiy, A., Van den Eynde, G., & Labeau, P. E. (2017). Nuclear data uncertainty propagation to integral responses using SANDY. *Annals of Nuclear Energy*, *101*, 359–366. https://doi.org/10.1016/j.anucene.2016.11.026

Glaeser, H., Luther, W., & Krzykacz-Hausmann, B. (2008). Methodenentwicklung und exemplarische Anwendungen zur Bestimmung der Aussagesicherheit von Rechenprogrammergebnissen. *GRS Report*, *GRS-A-3443*.

Glaeser, Horst. (2008). GRS method for uncertainty and sensitivity evaluation of code results and applications. *Science and Technology of Nuclear Installations*, *2008*. https://doi.org/10.1155/2008/798901

Hursin, M., Czifrus, S., Vanyi, A., Janik, J., Belgya, T., Perin, Y., Muzio, S. lo, Zert, J., Jantzen, L., Barbera, C., Pungerčič, A., Ambrožič, K., Vasiliev, A., Martino, flavio de, Tuominen, R., & Laurila, E. (2026). D2 . 2 – Description of the conventional and advanced models of the EVEREST research reactors. *EVEREST Delivrable*, *2.2*, 1–62.

Vanyi, A. (2023). *Experimental and numerical multi-physics analysis for the BME Training Reactor*. PhD thesis, Budapest University of Technology and Economics.

Zhu, T., Vasiliev, A., Ferroukhi, H., & Pautz, A. (2015). NUSS: A tool for propagating multigroup nuclear data covariances in pointwise ACE-formatted nuclear data using stochastic sampling method. *Annals of Nuclear Energy*, *75*, 713–722. https://doi.org/10.1016/j.anucene.2014.09.013

Funded by the European Union

Funded by the European Union. Views and opinions expressed are however those of the author(s) only and do not necessarily reflect those of the European Union or the European Atomic Energy Community ('EC-Euratom'). Neither the European Union nor the granting authority can be held responsible for them.